

# Can a secluded self-interacting dark sector generate detectable gravitational waves ?

Song Li,<sup>1,\*</sup> Jin Min Yang,<sup>1,2,3,†</sup> Mengchao Zhang,<sup>4,‡</sup> Yang Zhang,<sup>1,§</sup> and Rui Zhu<sup>2,3,¶</sup>

<sup>1</sup>*School of Physics, Henan Normal University, Xinxiang 453007, P. R. China*

<sup>2</sup>*Institute of Theoretical Physics, Chinese Academy of Sciences, Beijing 100190, P. R. China*

<sup>3</sup>*School of Physics, University of Chinese Academy of Sciences, Beijing 100049, P. R. China*

<sup>4</sup>*Department of Physics and Siyuan Laboratory,  
Jinan University, Guangzhou 510632, P. R. China*

## Abstract

In this work we study the possibility to detect the gravitational waves generated by a secluded self-interacting dark sector. “Secluded” means that the dark sector has almost no portal to the visible sector and thus its entropy is conserved by itself, and “self-interacting” means that dark matter in this model has a significant interaction to itself, making it consistent with the small-scale structure observations. A spontaneously broken  $U(1)'$  is introduced for the interactions in the dark sector, and nearly massless dark radiation is also introduced to avoid the over-closure problem. Through a parameter space scan, we find that this model is highly constrained by the current observed effective number of neutrinos ( $N_{\text{eff}}$ ) and the large-scale structure observable Lyman- $\alpha$ . Combined together, these two constraints make such a secluded self-interacting dark sector almost impossible to generate gravitational waves accessible at future projects like SKA or LISA.

---

\* [chunglee@htu.edu.cn](mailto:chunglee@htu.edu.cn)

† [jmyang@itp.ac.cn](mailto:jmyang@itp.ac.cn)

‡ Corresponding author: [mczhang@jnu.edu.cn](mailto:mczhang@jnu.edu.cn)

§ [zhangyangphy@zzu.edu.cn](mailto:zhangyangphy@zzu.edu.cn)

¶ Corresponding author: [zhurui@itp.ac.cn](mailto:zhurui@itp.ac.cn)

## CONTENTS

<b>I</b>	<b>Introduction</b>	<b>3</b>
<b>II</b>	<b>Dark sector model and its evolution</b>	<b>4</b>
A	Lagrangian of a secluded dark sector . . . . .	5
B	Evolution of the secluded dark sector . . . . .	6
<b>III</b>	<b>Calculation of observables and constraints of the self-interacting secluded dark sector</b>	<b>9</b>
A	DM self-interacting inside halos . . . . .	9
B	Dark acoustic oscillations (DAO) caused by the DM-DR scattering . . . . .	10
C	Contribution of DR to $N_{\text{eff}}$ . . . . .	12
D	GWs signals from dark sector FOPT . . . . .	12
<b>IV</b>	<b>Parameter space scan results</b>	<b>17</b>
<b>V</b>	<b>Conclusion</b>	<b>20</b>
	<b>References</b>	<b>20</b>

## I INTRODUCTION

The existence of dark matter (DM) has been confirmed by its gravitational effect [1, 2]. The abundance of DM in the universe has also been accurately determined by cosmological observations [2]. In the  $\Lambda$ CDM model, DM is assumed to be cold and collisionless, which is consistent with cosmological observations at large scale [3, 4]. However, the assumption of collisionless is challenged at smaller scales ( $\lesssim \mathcal{O}(\text{Mpc})$ ), i.e. the so called small-scale problems [5–12]. A series of studies have shown that a velocity-dependent cross-section between DMs can solve the small scale problems to a large extent [13–36]. Specifically, if the scattering cross-section between DMs inside halo is large enough, the evolution history and density distribution of DMs in the halo will be different from those of collisionless DM, and thus be in better agreement with astronomical observations. This requirement for DM property has inspired many model building works [37–65], and many of them introduce a light mediator particle and use it to induce the velocity-dependent cross-section between DMs. This light mediator is generally not massless, and thus, due to the limited force range, the success of cold DM on large scale will not be ruined.

It has been shown by previous studies that, in order to be consistent with small scale data, the masses of DM and light mediator should be located in  $\mathcal{O}(10)$  GeV –  $\mathcal{O}(100)$  GeV and  $\mathcal{O}(1)$  MeV –  $\mathcal{O}(10)$  MeV respectively. The existence of MeV scale dark mediator cause many problems. The dark mediator is generally chosen to be spin-0 scalar or spin-1 vector. Therefore, there are renormalizable portals that link dark sector to visible sector, i.e. Higgs portal or kinetic mixing. If the MeV scale dark mediators were populated in the early universe, then, because MeV scale is closed to Big Bang nucleosynthesis (BBN) temperature, the decay of these dark mediators will definitely affect BBN observables [66–68]. If dark mediators are very long-lived, it will also affect cosmic microwave background (CMB). Combined with other limits like supernova [69], direct detection [70], and rare hadron decay measurement [71], these MeV scale dark mediators are highly constrained.

A popular method used in the literature to evade above constraints is turning off those portals or assuming those portals to be negligibly small, and thus there is no visible energy injection from dark mediator during BBN or CMB period. On the other hand, to avoid overclosure problem, in the dark sector we also need to introduce some nearly massless particles to which dark mediators can decay [72]. Those nearly massless dark sector particles are generally called dark radiation (DR). Such a “DM+dark mediator+DR” scenario with self-interaction can easily escape traditional DM search limits (i.e., direct searches, indirect searches, and collider searches) and meet the DM properties observed on different scales. However, due to the lack of portal between dark sector and visible sector, the detection of this scenario is also difficult.

In recent years, stochastic gravitational waves (GWs) detection of new physics models are intensively studied, which can serve as a good method to detect the dark sector [42, 73–99]. If a first order phase transition (FOPT) ever happened in the dark sector, then a certain amount of latent heat will transfer

to GWs. After being produced, GWs propagate and get red-shifted in the universe, and thus its relic might be detected by current or future GWs detectors.

When investigating the application of stochastic GWs to detect this secluded “DM+dark mediator+DR” self-interacting scenario, even the portal to visible sector is negligibly small, there are two constraints that must be taken into account:

- In order to prevent the dark sector GWs from being too weak, the temperature of the dark sector (or says the temperature of DR) can not be too low. In addition, to enhance the GWs signals, the dark sector phase transition usually needs to be strongly super-cooling. However, in the strongly super-cooling case, the entropy released from the energy difference between false vacuum and true vacuum finally goes to the DR. DR as relativistic degree of freedom in addition to the SM neutrinos, will cause a deviation of the observed effective number of neutrinos ( $N_{\text{eff}}$ ). Therefore, the GWs detection of the “DM+dark mediator+DR” scenario inevitably encounters the constraint from  $N_{\text{eff}}$  measurement [78, 100].
- When the temperature of the DR is not very low, the DMs in the DR bath come through frequent scattering with the DR. This DM-DR scattering will cause the amplitude of perturbations to be suppressed at small scales. Since this phenomenon is similar to baryon acoustic oscillations (BAO) caused by baryon-photon scattering, it is also called dark acoustic oscillations (DAO) in the literature [101–103]. DAO will leave observable impact on matter power spectrum and cosmic microwave background (CMB), which in turn limits dark sector model with DR and self-interaction.

In this paper we propose a concrete but economical model to realize this “DM+dark mediator+DR” scenario. A dark  $U(1)'$  gauge symmetry is introduced to provide self-interaction in the dark sector, with both DM and DR charged by it. Furthermore, this dark  $U(1)'$  is spontaneously broken by a dark Higgs mechanism, and the corresponding FOPT process generates stochastic GWs. By analyzing DM self-scattering cross section inside halo, the stochastic GWs signal, the modification of  $N_{\text{eff}}$ , and the DAO, we conducted a comprehensive phenomenological study of this secluded dark sector model which is difficult to detect by traditional methods.

In Sec. II we introduce the dark sector model in our study. The evolution of the dark sector as the universe cools will also be described in this section. In Sec. III we explain in detail how various observables or limits are calculated. A comprehensive scan of the model parameter space and the presentation of results will be given in Sec. IV. We conclude this work in Sec. V.

## II DARK SECTOR MODEL AND ITS EVOLUTION

In this section we introduce a concrete dark sector model that can embrace all the phenomena introduced in Sec. I, and discuss how the temperature in this dark sector changes as the universe

evolves.

## A Lagrangian of a secluded dark sector

In the work we consider a secluded dark sector gauged by a  $U(1)'$  that induce the interaction inside dark sector. The ‘‘DM+dark mediator+DR’’ scenario can be embed in it. Similar models see also [42, 104–106]. The complete Lagrangian of the dark sector is following ((−, +, +, +) metric):

$$\mathcal{L}_{\text{Dark}} = \bar{\chi}(i\not{D} - m_\chi)\chi - (D_\mu S)^\dagger D^\mu S - (D_\mu \psi)^\dagger D^\mu \psi - \frac{1}{4}F'_{\mu\nu}F'^{\mu\nu} - V(S, \psi) \quad (1)$$

Here  $\chi$ , as vector-like fermion, is the DM particle.  $S$  is the complex dark Higgs field that obtain vacuum expectation value (VEV) below the critical temperature and break  $U(1)'$ . Complex scalar  $\psi$  is the lightest particle in the dark sector and will serve as DR.  $D_\mu \equiv \partial_\mu + ig'Q_i A'_\mu$  ( $i = \chi, S, \psi$ ) is the covariant derivative, and  $g'$  is the gauge coupling for  $U(1)'$ .  $F'_{\mu\nu} \equiv \partial_\mu A'_\nu - \partial_\nu A'_\mu$  is the field strength of  $U(1)'$  gauge boson  $A'$ .  $A'$  is also called dark photon. Different with the SM photon, dark photon  $A'$  becomes massive after the spontaneous symmetry breaking (SSB) of  $U(1)'$ .

The  $U(1)'$  charge assignment can be quite arbitrary. In this work we simply let the  $U(1)'$  charge to be  $\{Q_\chi, Q_S, Q_\psi\} = \{+1, +2/3, +1\}$ . Other charge assignment will not change the analysis too much <sup>1</sup>. Under this charge assignment, the complete dark scalar potential is given by:

$$V(S, \psi) = \tilde{m}_\psi^2 \psi^\dagger \psi - \mu^2 S^\dagger S + \frac{\lambda_S}{4} (S^\dagger S)^2 + \frac{\lambda_\psi}{4} (\psi^\dagger \psi)^2 + \lambda_{S\psi} (S^\dagger S) (\psi^\dagger \psi) \quad (2)$$

After  $U(1)'$  SSB,  $S$  obtains VEV, i.e.  $\langle S \rangle = v/\sqrt{2}$  with  $v \equiv 2\mu/\sqrt{\lambda_S}$ . Then the mass square of  $\psi$  becomes  $m_\psi^2 \equiv \tilde{m}_\psi^2 + \frac{1}{2}\lambda_{S\psi}v^2$ . To make  $\psi$  a DR, we simply require  $m_\psi^2 \ll (0.1 \text{ eV})^2$ . In addition, dark Higgs mass square  $m_s^2 = \frac{1}{2}\lambda_S v^2$  and dark photon mass square  $m_{A'}^2 = (\frac{2}{3}g')^2 v^2$  are also fixed after SSB. The value for coupling  $\lambda_\psi$  and  $\lambda_{S\psi}$  are not so relevant in this work, and thus the input parameters of this model are:

$$m_\chi, m_{A'}, m_s, g' \text{ (or } \alpha'), \quad (3)$$

where  $\alpha' \equiv \frac{g'^2}{4\pi}$  is the dark fine structure constant.

The parameter range we will study is as follows

$$10 \text{ GeV} < m_\chi < 600 \text{ GeV}, \quad 0.1 \text{ MeV} < m_{A'} < 10 \text{ MeV}, \quad 0.005 < \alpha' < 0.4 \quad (4)$$

$$\sqrt{\frac{\alpha' m_{A'}^2}{3\pi}} < m_s < \frac{1}{2} m_{A'} \quad (5)$$

Parameter ranges in the first line is favored by the small-scale structure, as we briefly explained in Sec. I. More detail will be given in following sections. We set  $\alpha'$  greater than 0.005 to make the DM relic

<sup>1</sup> If one consider other issues like asymmetry generation in the dark sector, or the  $\chi - \bar{\chi}$  oscillation,  $U(1)'$  charge assignment will be a subtle problem. See, e.g. [42, 84, 107, 108], for more discussion.

density easy to satisfy, see next subsection for explanation.  $\alpha' < 0.4$  is simply used to avoid Landau pole at a high energy scale [109]. The lower bound of dark Higgs mass  $m_s$  is the Linde-Weinberg bound which says  $m_s$  can not be too light otherwise the SSB can not happen when loop corrections to effective potential are considered. The lower bound present here is an approximation, while the complete formula can be found in our previous paper [109]. The upper bound of  $m_s$  is required by a FOPT in the dark sector. Lattice simulations show that FOPT in Abelian Higgs model can only happen when Higgs mass is smaller or much smaller than gauge boson mass [110, 111]. Thus we dictate this upper bound to make our model has the potential to generate detectable stochastic gravitational waves from a FOPT.

It should be noticed that our dark sector model have three renormalizable portals to the visible sector, i.e.  $(S^\dagger S)(H^\dagger H)$ ,  $(\psi^\dagger \psi)(H^\dagger H)$ , and  $F'_{\mu\nu} F'^{\mu\nu}$ , with  $H$  the SM Higgs doublet and  $F'^{\mu\nu}$  the electromagnetic field strength. In this work we set the coupling factors of these three terms to be zero and thus make the dark sector fully secluded.

## B Evolution of the secluded dark sector

In this work we assume the dark sector to be thermalized at a very high temperature. This thermalization process in the dark sector can also be called dark reheating. In this work we use  $T'$  to label the temperature of dark sector. The evolution of the dark sector after dark reheating is roughly as follows

- Dark reheating temperature  $T'_{\text{reh}}$  is much larger than the mass of dark matter, i.e.  $T'_{\text{reh}} \gg m_\chi$ . Thus all the dark sector particles we listed in the last subsection are highly relativistic after dark reheating, for a period of time. Effective degrees of freedom (d.o.f.) for energy density in the dark sector (labeled as  $g'_{\star,e}$ ) right after dark reheating is  $g'_{\star,e}(T'_{\text{reh}}) = \frac{7}{8} \times 4 + 2 + 2 + 2 = 9.5$ .
- As the temperature drops, DM  $\chi$  and anti-DM  $\bar{\chi}$  gradually becomes non-relativistic and their abundances decreases through the annihilation process  $\chi\bar{\chi} \rightarrow A'A'$ . After freeze-out, the sum of DM abundance and anti-DM abundance  $Y_\chi + Y_{\bar{\chi}}$  is frozen and it constitutes the observed relic density.

In the symmetric DM case where  $Y_\chi = Y_{\bar{\chi}}$ , the relic density is inversely proportional to annihilation cross-section  $\sigma_{\chi\bar{\chi} \rightarrow A'A'}$ , and thus the available parameter space is greatly compressed. To enlarge the parameter space, we assume there is an asymmetry between DM and anti-DM, i.e.  $Y_{\Delta\chi} \equiv Y_\chi - Y_{\bar{\chi}} > 0$ . It has been shown in our previous work that when  $\alpha' > 0.005$ , the relic density is mainly determined by  $Y_{\Delta\chi}$  [42]. Our work [42] also shows that  $Y_{\Delta\chi}$  can vary over a wide range in a complete model (this is mainly because CP violation phase in the dark sector can be quite large) and thus relic density can always be satisfied. Related discussion also see, e.g. [112, 113].

- When  $T'$  is around MeV scale, the FOPT happens in the dark sector and dark photon  $A'$  becomes massive. Bubble collision and subsequent processes generate stochastic gravitational waves which might be detectable. Released latent heat also heat up the dark sector. When the FOPT lasts much shorter than the Hubble time (this is actually always true in our dark sector model), we can expect energy density is approximately conserved before and after FOPT:

$$u'_{\text{before}} = u'_{\text{after}}, \quad (6)$$

where  $u'$  represents the internal energy density of the dark sector.  $u'$  can be calculated from the effective potential in thermal equilibrium:

$$u' = V(v, T) + sT = V(v, T) - T \frac{\partial V(v, T)}{\partial T}. \quad (7)$$

We can use the percolation temperature  $T'_{\text{perc}}$  (the temperature at which FOPT is nearly complete) as  $T'_{\text{before}}$  to calculate  $T'_{\text{after}}$ , with the corresponding equation being:

$$V(0, T'_{\text{perc}}) - T \frac{\partial V(0, T)}{\partial T} \Big|_{T=T'_{\text{perc}}} = V(v(T'_{\text{after}}), T'_{\text{after}}) - T \frac{\partial V(v, T)}{\partial T} \Big|_{\substack{T=T'_{\text{after}} \\ v=v(T'_{\text{after}})}} \quad (8)$$

Another method for calculating the internal energy density is through effective degrees of freedom and the zero-temperature effective potential:

$$u' \approx V(v, T=0) + \rho' = V(v, T=0) + g'_{\star, e} \frac{\pi^2}{30} T^4 \quad (9)$$

Therefore, Eq. (6) can be approximated as:

$$\rho'_{\text{after}} = \rho'_{\text{before}} + \Delta V(v, T=0) \quad (10)$$

with  $\Delta V(v, T=0)$  the vacuum energy difference between two phases and  $\rho'$  the radiation energy density in the dark sector. Above equation is used in previous studies like [114]. It is clear that the reheating after the phase transition mainly comes from the release of vacuum energy, which increases the temperature of the dark sector by a factor of approximately  $\left(1 + \frac{\Delta V}{\rho'_{\text{before}}}\right)^{1/4}$ , provided  $g'_{\star, e}$  doesn't change much during FOPT. This result helps us quickly estimate the reheating effect, but in this work we will use the more precise formula Eq. (8) to calculate  $T'_{\text{after}}$ .

- After FOPT, as the dark sector temperature decreases, the remaining massive  $A'$  and  $s$  will all eventually decay to DR via  $A' \rightarrow \psi\psi^\dagger$  and  $s \rightarrow \psi\psi^\dagger$  processes. Then the dark sector will be composed by DM  $\chi$  and DR  $\psi/\psi^\dagger$ . Dark sector d.o.f.  $g'_\star$  during that time is 2.

It will be convenient to define a temperature ratio between dark sector and visible sector:

$$\xi \equiv \frac{T'}{T_\gamma} \quad (11)$$

Here is  $T_\gamma$  is the photon temperature in the visible sector. We can consider temperature ratio  $\xi$  as a function of  $T_\gamma$ , i.e.  $\xi(T_\gamma)$ . The value of  $\xi$  right after dark reheating (to be labeled as  $\xi_{\text{reh}}$ ) is actually an input parameter that depends on the detail of very early universe. The value of  $\xi(T_\gamma)$  can be determined by the entropy conservation (note the jump during FOPT):

$$\xi(T_\gamma) = \begin{cases} \xi_{\text{reh}} \left( \frac{9.5 \times g_{\star,s}(T_\gamma)}{106.75 \times g'_{\star,s}(T_\gamma \xi)} \right)^{\frac{1}{3}}, & \text{before FOPT;} \\ \xi_{\text{after}} \left( \frac{g'_{\star,s}(T'_{\text{after}}) \times g_{\star,s}(T_\gamma)}{g_{\star,s}(T'_{\text{after}}/\xi_{\text{after}}) \times g'_{\star,s}(T_\gamma \xi)} \right)^{\frac{1}{3}}, & \text{after FOPT,} \end{cases} \quad (12)$$

with  $g_{\star,s}$  and  $g'_{\star,s}$  the effective d.o.f. for entropy density in the visible sector and dark sector, respectively. In dark sector, approximation  $g'_{\star,s} \approx g'_{\star,e}$  is always holds true. While in the visible sector,  $g_{\star,s} \approx g_{\star,e}$  is valid only before neutrino decoupling. Effective d.o.f. in both sectors can be determined numerically, see [115] for detailed formula.

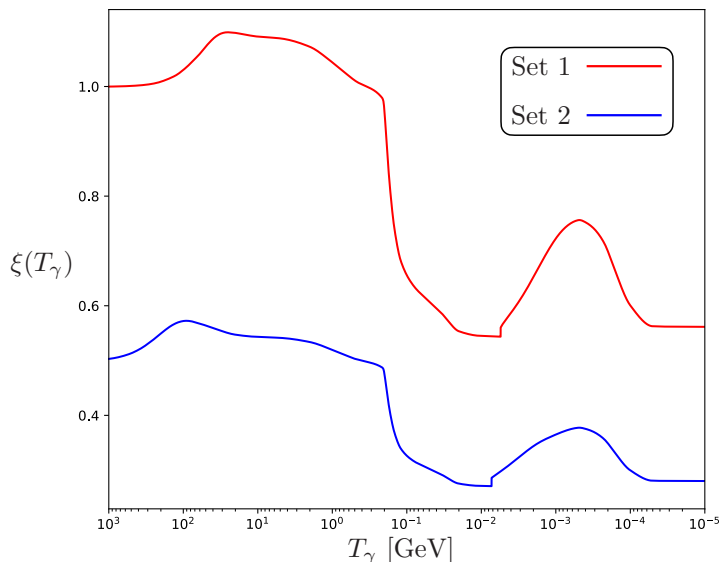


FIG. 1. Temperature ratio  $\xi$  as functions of  $T_\gamma$  for two benchmark sets.

To illustrate the evolution of  $\xi$ , we consider following two benchmark sets:

$$\text{Set 1: } m_\chi = 200 \text{ GeV, } m_{A'} = 5 \text{ MeV, } m_s = 2 \text{ MeV, } \alpha' = 0.2, \xi_{\text{reh}} = 1.0$$

$$\text{Set 2: } m_\chi = 400 \text{ GeV, } m_{A'} = 4 \text{ MeV, } m_s = 1 \text{ MeV, } \alpha' = 0.1, \xi_{\text{reh}} = 0.5$$

Here  $T'_{\text{perc}}$  is the percolation temperature which roughly marks the completion of the dark FOPT.  $T'_{\text{perc}}$  will be explained in detail in Sec. III. In Fig. 1 we present the temperature ratio  $\xi$  as functions of  $T_\gamma$  for above two benchmark sets. As we discussed before, FOPT happens at  $T'_{\text{perc}}$  (around  $\mathcal{O}(1)$  MeV) instantly increases the value of  $\xi$ . On the other hand, when  $T_\gamma \ll \text{MeV}$ ,  $\xi$  will approach its asymptotic value. The asymptotic value of  $\xi$  will be labeled as  $\xi_\infty$  and plays an important role in the calculation of the next section.

### III CALCULATION OF OBSERVABLES AND CONSTRAINTS OF THE SELF-INTERACTING SECLUDED DARK SECTOR

In this section we present in detail the calculations of the observables and constraints of the dark sector, including DM scattering cross section inside halos, DAO caused by the DM-DR scattering, the additional contribution to  $N_{\text{eff}}$ , and FOPT induced GWs spectrums.

#### A DM self-interacting inside halos

The behavior of DM inside halos, such as the density distribution of DM or their rotation curves, depend on the average scattering cross section between DMs over DM mass,  $\bar{\sigma}/m_\chi$ . Due to the Virial theorem, different astronomical systems (from dwarf galaxies to galaxy clusters) with different masses have different average DM relative velocities  $\langle v_{\text{rel}} \rangle$ . In order for DMs in different astronomical systems to behave as observed,  $\bar{\sigma}/m_\chi$  needs to depend on the average velocity  $\langle v_{\text{rel}} \rangle$ . Below we summarize  $\langle v_{\text{rel}} \rangle$  of different astronomical systems and the requirements for  $\bar{\sigma}/m_\chi$  from different observables:

- Diversity of galactic rotation curves for isolated spiral galaxies over a wide mass range [116–118]:

$$\langle v_{\text{rel}} \rangle \sim 43.2 - 432 \text{ km/s} , \bar{\sigma}/m_\chi > 2 \text{ cm}^2 \text{ g}^{-1} \quad (13)$$

- To avoid subhalo evaporation of Milky Way (MW) size halo [19, 21, 31]:

$$\langle v_{\text{rel}} \rangle \gtrsim 200 \text{ km/s} , \bar{\sigma}/m_\chi < 10 \text{ cm}^2 \text{ g}^{-1} \quad (14)$$

- The anti-correlation between the central DM densities and orbital pericenter distances of Milky Way’s dwarf spheroidal galaxies (MW dSphs) [119]:

$$\langle v_{\text{rel}} \rangle \sim 20 - 60 \text{ km/s} , \bar{\sigma}/m_\chi \sim \mathcal{O}(10) - \mathcal{O}(100) \text{ cm}^2 \text{ g}^{-1} \quad (15)$$

Detailed values are given in Tab. I.

- Dense DM substructure which perturbs the strong lens galaxy SDSSJ0946+1006 [120, 121]:

$$\langle v_{\text{rel}} \rangle \sim 144 \text{ km/s} , \bar{\sigma}/m_\chi \sim 14 - 25 \text{ cm}^2 \text{ g}^{-1} \quad (16)$$

This observation is labeled as ‘perturber’ in Tab. I.

- Rotation curves of isolated and gas-rich ultradiffuse galaxies (UDGs) [121]<sup>2</sup>:

$$\langle v_{\text{rel}} \rangle \sim 57.6 \text{ km/s} , \bar{\sigma}/m_\chi \sim 47 - 86 \text{ cm}^2 \text{ g}^{-1} \quad (17)$$

---

<sup>2</sup> The lower bound comes from private discussion with the author of Ref. [121].

Observables	$\langle v_{\text{rel}} \rangle$ (km/s)	$\bar{\sigma}/m_\chi$ (cm <sup>2</sup> /g)
MW dSph: UM	30.87	40 – 50
MW dSph: Draco	56.34	20 – 30
MW dSph: LeoII	20.98	90 – 150
MW dSph: Sextans	32.34	70 – 120
MW dSph: Carina	48.42	40 – 50
MW dSph: CVnI	38.29	50 – 80
MW dSph: Sculptor	62.83	30 – 40
MW dSph: Fornax	57.95	30 – 50
MW dSph: LeoI	58.27	50 – 70
Perturber	144	14 – 25
UDGs	57.6	47 – 86

TABLE I. Small-scale data used for  $\chi^2$  fit.

- For groups and clusters with  $\langle v_{\text{rel}} \rangle$  about 1152 km/s and 1440 km/s,  $\bar{\sigma}/m_\chi$  need to be smaller than 1 cm<sup>2</sup>g<sup>-1</sup> and 0.1 cm<sup>2</sup>g<sup>-1</sup> to be consistent with observations [14, 23, 34].

In Tab. I we present all the data with an error bar of  $\bar{\sigma}/m_\chi$ . These data will be used to perform a  $\chi^2$  fit to obtain the corresponding  $2\sigma$  region in parameter space which is consistent with small-scale observations. Constraints other than those listed in Tab. I is used to limit the parameter space directly.

The methods of calculating DM scattering cross-section depend on model parameters  $\{m_\chi, m_{A'}, \alpha'\}$  and  $v_{\text{rel}}$ . In the Born regime with  $\frac{\alpha' m_\chi}{m_{A'}} \ll 1$ , analytic formula can be obtained via perturbative calculation [41, 44, 63, 122]. In the classical regime with  $\frac{\alpha' m_\chi}{m_{A'}} \gtrsim 1$  and  $\frac{m_\chi v_{\text{rel}}}{m_{A'}} \gg 1$ , formula are obtained via fitting with numerical results [41, 44, 123, 124]. In the quantum regime with  $\frac{\alpha' m_\chi}{m_{A'}} \gtrsim 1$  and  $\frac{m_\chi v_{\text{rel}}}{m_{A'}} \lesssim 1$ , cross-section can be calculated via Hulthén approximation [63]. In the semi-classical regime  $\frac{\alpha' m_\chi}{m_{A'}} \gtrsim 1$  and  $\frac{m_\chi v_{\text{rel}}}{m_{A'}} \gtrsim 1$ , analytic formula is also given in [125]. We use viscosity cross section  $\sigma_V \equiv \int d\Omega \sin^2 \theta \frac{d\sigma}{d\Omega}$  as the proxy of DM elastic scattering. As suggested by [125],  $\bar{\sigma} \equiv \langle \sigma_V v_{\text{rel}}^3 \rangle / 24 \sqrt{\pi} v_0^3$ , with  $v_0$  the velocity dispersion, is used to do the thermal averaging. Above results have been implemented in public package CLASSICS [125], and we will use it to calculate  $\bar{\sigma}$  in this work.

## B Dark acoustic oscillations (DAO) caused by the DM-DR scattering

The relic in the dark sector contain not only stable DM  $\chi$ , but also stable DR  $\psi$ . The scattering between DM and DR induce pressure in the dark plasma, and thus erase the matter perturbation at small scale. That is to say, compared with the traditional cold DM, the matter power spectrum in our dark sector model will be suppressed in the high- $k$  region, which will affect the structure formation

and leave imprint on CMB [101–103].

To handle the impact from the DM-DR scattering, here we use the ETHOS (effective theory of structure formation) parameterization to simplify our analysis [124]. In the ETHOS framework, we only need to know the interaction strength bwtween DR and DM (labeled by  $a_{\text{dark}}$ ), the dependence of the comoving interaction rate of DR and DM (labeled by  $\Gamma_{\text{DR-DM}}$ ) on dark sector temperature  $T'$ <sup>3</sup>, and the energy density of DR (described by temperature ratio  $\xi_\infty$ ). Because the perturbation grows slowly before matter dominated period, by that time  $\xi$  has already reached its asymptotic value  $\xi_\infty$ . The comoving interaction rate  $\Gamma_{\text{DR-DM}}$  is given by

$$\Gamma_{\text{DR-DM}} = \left( \frac{3\bar{n}_\chi m_\chi}{4\rho_{\text{DR}}} \right) \frac{a(T')}{16\pi m_\chi^3} \frac{\eta_{\text{DR}}}{3} \int \frac{p^2 dp}{2\pi^2} p^2 \frac{\partial \bar{f}_{\text{DR}}(p)}{\partial p} [A_0(p) - A_1(p)] , \quad (18)$$

with  $\bar{n}_\chi$ ,  $\rho_{\text{DR}}$ ,  $a(T')$ , and  $\bar{f}_{\text{DR}}(p)$  the averaged DM number density, DR energy density, scale factor, and averaged DR phase-space density with temperature  $T'$ , respectively.  $\eta_i$  is the inner d.o.f. of particle  $i$ . Functions  $A_i(p)$  are given by

$$A_l(p) = \frac{1}{2} \int_{-1}^1 d\tilde{\mu} P_l(\tilde{\mu}) \left( \frac{1}{\eta_\chi \eta_{\text{DR}}} \sum_{\text{states}} |\mathcal{M}|^2 \right) \Big|_{\substack{t=2p^2(\tilde{\mu}-1) \\ s=m_\chi^2+2pm_\chi}} \quad (19)$$

with  $|\mathcal{M}|^2$  the amplitude square of DM-DR scattering process  $\chi\psi \rightarrow \chi\psi$ .  $P_l(\tilde{\mu})$  is the Legendre polynomial and  $\tilde{\mu}$  is the cosine of the angle between the incident and scattered particles.

In our model, the scattering of DM and DR occurs by exchanging a t-channel  $A'$ , and the corresponding summed amplitude square is

$$\sum_{\text{states}} |\mathcal{M}|^2 = 32g'^4 \frac{pm_\chi(pm_\chi + p^2(\tilde{\mu} - 1))}{(2p^2(\tilde{\mu} - 1) - m_{A'}^2)^2} \approx 32g'^4 \frac{p^2 m_\chi^2}{m_{A'}^4} , \text{ for } p \ll m_{A'} < m_\chi . \quad (20)$$

Thus,

$$A_0(p) = \frac{32g'^4}{\eta_\chi \eta_{\text{DR}}} \frac{p^2 m_\chi^2}{m_{A'}^4} , \quad A_1(p) = 0 \quad (21)$$

Integrating with respect to  $p$ , we get

$$\Gamma_{\text{DR-DM}} = -a(T') \frac{4\pi^3}{21} \frac{\bar{n}_\chi}{\rho_{\text{DR}}} \frac{g'^4 T'^6}{\eta_\chi m_{A'}^4} = -\frac{40\pi}{7} \frac{\rho_{\chi,0}}{\eta_{\text{DR}} \eta_\chi} \frac{g'^4}{(\xi_\infty T_{\text{CMB},0})^2} \frac{T'^4}{m_\chi m_{A'}^4} \quad (22)$$

Here  $\rho_{\chi,0}$  is current DM energy density and  $T_{\text{CMB},0}$  is current CMB temperature. By this expression we know that  $\Gamma_{\text{DR-DM}} \propto T'^4$ . On the other hand, the value of interaction strength  $a_{\text{dark}}$  can be induced from  $\Gamma_{\text{DR-DM}}$  via

$$\Gamma_{\text{DR-DM}} = -\Omega_\chi h^2 a_{\text{dark}} \left( \frac{1+z}{1+z_d} \right)^4 \quad (23)$$

<sup>3</sup>  $\Gamma_{\text{DR-DM}} \propto T'^n$ , and thus this dependence is described by the value of  $n$ .

with  $z_d = 10^7$  a normalization factor. Noting  $1 + z = T'/(\xi_\infty T_{\text{CMB},0})$ , we can get an expression of  $a_{\text{dark}}$  that is convenient for our model

$$a_{\text{dark}} = \frac{40\pi \times 10^{28} \times g'^4}{7\eta_{\text{DR}}\eta_\chi m_\chi m_{A'}^4} (\rho_{\text{crit},0} h^{-2}) (\xi_\infty T_{\text{CMB},0})^2 = 3.07 \times 10^7 \times \xi_\infty^2 g'^4 \left(\frac{\text{GeV}}{m_\chi}\right) \left(\frac{\text{MeV}}{m_{A'}}\right)^4 \text{Mpc}^{-1} \quad (24)$$

The bound on  $a_{\text{dark}}$  strongly relate to the dependence of  $\Gamma_{\text{DR-DM}}$  on  $T'$ . For  $\Gamma_{\text{DR-DM}} \propto T'^4$ , the most stringent restriction on  $a_{\text{dark}}$  currently comes from Lyman- $\alpha$  [126]:

$$a_{\text{dark}} < 30 \xi_\infty^{-4} \text{Mpc}^{-1} \quad (25)$$

Thus this constrain becomes weaker when temperature ratio  $\xi_\infty$  is smaller than 1.

### C Contribution of DR to $N_{\text{eff}}$

$\Delta N_{\text{eff}}$  is the effective number of neutrino species in addition to the SM neutrinos, and in our model it come from DR  $\psi/\psi^\dagger$ . The calculation of  $\Delta N_{\text{eff}}$  is straightforward:

$$\Delta N_{\text{eff}} = \frac{8}{7} \left(\frac{T_\nu}{T_\gamma}\right)^{-4} \frac{\rho_{\text{DR}}}{\rho_\gamma} = \frac{8}{7} \left(\frac{4}{11}\right)^{-4/3} \left(\frac{2}{2}\right) \left(\frac{T'}{T_\gamma}\right)^4 = \frac{8}{7} \left(\frac{4}{11}\right)^{-4/3} \xi_\infty^4 \quad (26)$$

Compared with our previous work [42], the above equation also takes into account the dark sector heating caused by FOPT, as we discussed in Sec. II B.

Current limit on  $\Delta N_{\text{eff}}$  from joint Planck + BAO data analysis [2] and precise SM calculation [127] is:

$$\Delta N_{\text{eff}} < 0.29 \quad (27)$$

Thus,  $\Delta N_{\text{eff}}$  gives a very strong bound on dark sector temperature and the strength of FOPT in the dark sector.

### D GWs signals from dark sector FOPT

In this subsection we briefly introduce the calculation process of GWs signals caused by the dark sector FOPT, and the formulas used will be shown. The FOPT happens around MeV scale, and thus the DM in our model, which is much heavier than MeV, is irrelevant in phase transition. Furthermore, DR  $\psi/\psi^\dagger$  is much lighter than MeV and have very tiny coupling with dark Higgs, and so DR can be ignored in the thermal effective potential. The relevant Lagrangian is actually an Abelian Higgs model [128, 129]:

$$\mathcal{L}_{U(1)'} = -(\partial_\mu S + iQ_S g' A'_\mu S)^\dagger (\partial^\mu S + iQ_S g' A'^\mu S) - \frac{1}{4} F'_{\mu\nu} F'^{\mu\nu} + \mu^2 S^\dagger S - \frac{\lambda_S}{4} (S^\dagger S)^2 \quad (28)$$

Under Landau gauge, ghost is decoupled, and the field value dependent mass squares for dark Higgs  $s$ , Goldstone  $a$ , and dark photon  $A'$ , are:

$$m_s^2(\phi) = \frac{3}{4}\lambda_S\phi^2 - \mu^2, \quad m_a^2(\phi) = \frac{1}{4}\lambda_S\phi^2 - \mu^2, \quad m_{A'}^2(\phi) = (Q_S g')^2\phi^2 \quad (29)$$

The thermal effective potential at temperature  $T$  (in this subsection the temperature of dark sector is labeled by  $T$  for convenience) is schematically expressed as <sup>4</sup>:

$$V(\phi, T) = V^0(\phi) + V^{1\text{-loop}}(\phi) + V^{\text{T}}(\phi, T) + V^{\text{daisy}}(\phi, T) \quad (30)$$

Here  $V^0$  is the tree-level potential,  $V^{1\text{-loop}}$  is the sum of one-loop Coleman-Weinberg potential with on-shell counter terms,  $V^{\text{T}}$  is thermal correction, and  $V^{\text{daisy}}$  is the thermal daisy resummation. Tree-level potential is directly given by:

$$V^0(\phi) = -\frac{1}{2}\mu^2\phi^2 + \frac{1}{16}\lambda_S\phi^4 \quad (31)$$

$V^{1\text{-loop}} = V^{\text{CW}} + \delta_{\text{c.t.}}$  with  $V^{\text{CW}}$  the one-loop Coleman-Weinberg potential [130]:

$$V^{\text{CW}}(\phi) = \frac{1}{64\pi^2} \left\{ m_s^4(\phi) \left[ \ln \left( \frac{m_s^2(\phi)}{Q^2} \right) - \frac{3}{2} \right] + m_a^4(\phi) \left[ \ln \left( \frac{m_a^2(\phi)}{Q^2} \right) - \frac{3}{2} \right] + 3m_{A'}^4(\phi) \left[ \ln \left( \frac{m_{A'}^2(\phi)}{Q^2} \right) - \frac{5}{6} \right] \right\} \quad (32)$$

The counter terms  $\delta_{\text{c.t.}}$  is added to make the one-loop potential satisfy following on-shell conditions:

$$\left. \frac{d}{d\phi} V^{1\text{-loop}}(\phi) \right|_{\phi=v} = 0, \quad \left. \frac{d^2}{d\phi^2} V^{1\text{-loop}}(\phi) \right|_{\phi=v} = -\Delta\Sigma \quad (33)$$

where  $\Delta\Sigma \equiv \Sigma(m_s^2) - \Sigma(0)$  is the difference of scalar self-energy.  $\Delta\Sigma$  is used to deal with the infrared (IR) divergence caused by massless Goldstone under Landau gauge [131]. Final expression of  $V^{1\text{-loop}}$  is [132]:

$$V^{1\text{-loop}}(\phi) = \frac{1}{64\pi^2} \left[ m_s^4(\phi) \left( \ln \frac{m_s^2(\phi)}{m_s^2} - \frac{3}{2} \right) + 2m_s^2 m_s^2(\phi) \right] + \frac{3}{64\pi^2} \left[ m_{A'}^4(\phi) \left( \ln \frac{m_{A'}^2(\phi)}{m_{A'}^2} - \frac{3}{2} \right) + 2m_{A'}^2 m_{A'}^2(\phi) \right] + \frac{1}{64\pi^2} \left[ m_a^4(\phi) \left( \ln \frac{m_a^2(\phi)}{m_s^2} - \frac{3}{2} \right) \right] \quad (34)$$

with  $m_{A'}$ ,  $m_a$ , and  $m_s$  the zero-temperature masses. Thermal correction is given by [133, 134]:

$$V^{\text{T}}(\phi, T) = \frac{T^4}{2\pi^2} \left[ J_B \left( \frac{m_s^2(\phi)}{T^2} \right) + J_B \left( \frac{m_a^2(\phi)}{T^2} \right) + 3J_B \left( \frac{m_{A'}^2(\phi)}{T^2} \right) \right] \quad (35)$$

<sup>4</sup> It should be emphasized that the  $V(v, T)$  used in Eq. (7) also include contribution from DR.

with bosonic thermal function:

$$J_B(x) = \int_0^\infty k^2 \ln \left[ 1 - \exp \left( -\sqrt{k^2 + x} \right) \right] dk \quad (36)$$

Finally, daisy resummation, which is used to solve the IR problem caused by the bosonic zero-mode, is given by [135]:

$$V^{\text{daisy}}(\phi, T) = -\frac{T}{12\pi} \left\{ \left[ (m_s^2(\phi) + \Pi_s(T))^{\frac{3}{2}} - (m_s^2(\phi))^{\frac{3}{2}} \right] \right. \\ \left. + \left[ (m_a^2(\phi) + \Pi_a(T))^{\frac{3}{2}} - (m_a^2(\phi))^{\frac{3}{2}} \right] + \left[ (m_{A'}^2(\phi) + \Pi_{A'}(T))^{\frac{3}{2}} - (m_{A'}^2(\phi))^{\frac{3}{2}} \right] \right\} \quad (37)$$

with  $\Pi_s(T) = (\lambda_S/6 + (Q_S g')^2/4) T^2$ ,  $\Pi_a(T) = (\lambda_S/6 + (Q_S g')^2/4) T^2$ , and  $\Pi_{A'}(T) = ((Q_S g')^2/3) T^2$  the thermal Debye mass squares.

### 1 Phase transition parameters

The most important parameter for the FOPT GWs signal calculation is the characteristic temperature for abundant GWs production,  $T_*$ . In the literature,  $T_*$  is generally taken to be the percolation temperature  $T_{\text{perc}}$ . Percolation temperature  $T_{\text{perc}}$  is determined by the temperature where the probability for a point in the false vacuum is 70% [136–143]:

$$P(T_{\text{perc}}) = e^{-I(T_{\text{perc}})} = 70\% , \quad I(T) = \frac{4\pi v_w^3}{3} \int_T^{T_c} \frac{dT' \Gamma(T')}{H(T') T'^4} \left( \int_T^{T'} \frac{d\tilde{T}}{H(\tilde{T})} \right)^3 \quad (38)$$

with  $v_w$  the bubble wall velocity,  $\Gamma(T)$  the phase transition rate per unit volume at temperature  $T$ ,  $H(T)$  the Hubble expansion rate, and  $T_c$  the critical temperature where two phases have the same free energy density. The determination of  $v_w$  will be discussed later on. The thermal transition rate  $\Gamma(T)$  is given by [144–146]:

$$\Gamma(T) = T^4 \left( \frac{S_3(T)}{2\pi T} \right)^{3/2} e^{-S_3(T)/T} \quad (39)$$

with 3-D Euclidean action  $S_3(T)$  is given by:

$$S_3(T) = \int d^3x \left[ \frac{1}{2} (\nabla\phi)^2 + V(\phi, T) \right] = 4\pi \int_0^\infty r^2 dr \left[ \frac{1}{2} \left( \frac{d\phi}{dr} \right)^2 + V(\phi, T) \right] \quad (40)$$

$\phi(r)$  is determined by equation of motion:

$$\frac{d^2\phi}{dr^2} + \frac{2}{r} \frac{d\phi}{dr} = \frac{\partial V(\phi, T)}{\partial\phi} \quad (41)$$

and boundary conditions  $\lim_{r \rightarrow \infty} \phi(r) = 0$  and  $\left. \frac{d\phi}{dr} \right|_{r=0} = 0$ . Equation of motion of  $\phi(r)$  can be solved numerically by shooting method [147–149].

After determining the phase transition temperature  $T_*$ , which is actually percolation temperature  $T_{\text{perc}}$ , other phase transition parameters that need to be calculated are FOPT strength parameter  $\mathbb{A}$ , duration parameter  $\beta/H_*$ , bubble wall velocity  $v_w$ , and efficiency parameters  $\kappa_{b,s,t}$ .

$\mathbb{A}$  is the difference of the trace of energy-momentum tensor between two phases divided by radiation energy density:

$$\mathbb{A} = \frac{1}{\rho_*} \left[ \Delta V - \frac{T}{4} \frac{d\Delta V}{dT} \right]_{T=T_*} \quad (42)$$

with  $\rho_*$  is the radiation energy density at  $T_*$ .  $\beta/H_*$  is given by:

$$\frac{\beta}{H_*} = T \left. \frac{d}{dT} \left( \frac{S_3(T)}{T} \right) \right|_{T=T_*} \quad (43)$$

To determine  $v_w$  and  $\kappa_{b,s,t}$ , first we need to confirm whether the FOPT is “runaway” or not. It will be convenient to define a dark sector strength parameter  $\mathbb{A}'$  which is given by  $\mathbb{A}' = \frac{\rho_*}{\rho'_*} \mathbb{A}$  with  $\rho'_*$  the radiation energy density in the dark sector.

If  $\mathbb{A}'$  is larger than the so-called threshold value  $\mathbb{A}'_\infty = \frac{1}{\rho'_*} \frac{T_*^2}{24} (\sum_i c_i n_i \Delta m_i^2)$  [150] ( $c_i = 1$  (1/2) for bosons (fermions),  $n_i$  is the number of d.o.f., and  $\Delta m_i^2$  the mass square difference between two phases), then FOPT is “runaway” and bubble wall velocity  $v_w$  can be approximated by 1<sup>5</sup>.  $\kappa_{b,s,t}$  are given by [152, 153]:

$$\kappa_b = 1 - \frac{\mathbb{A}'_\infty}{\mathbb{A}'}, \quad \kappa_s = \frac{\mathbb{A}'_\infty}{\mathbb{A}'}, \quad \kappa_t = 0.1\kappa_s \quad (44)$$

If  $\mathbb{A}' < \mathbb{A}'_\infty$ , then the FOPTP is “non-runaway” and bubble wall will eventually reach a subluminal velocity. Due to the difficulty in the calculation of  $v_w$  in this case [154–160], in this work we simply take  $v_w = 0.9$  for a quick and optimistic GWs signal estimation. In this case,  $\kappa_{b,s,t}$  are approximately given by [150]:

$$\kappa_b \simeq 0, \quad \kappa_s = \frac{\mathbb{A}'}{0.73 + 0.083\sqrt{\mathbb{A}' + \mathbb{A}'_\infty}}, \quad \kappa_t = 0.1\kappa_s \quad (45)$$

## 2 Gravitational waves spectrum

There are three main GWs generation mechanisms during FOPT: bubble walls collision [161–166], sound waves [152, 167–169], and magnetohydrodynamic turbulence [170–175]. The spectrum of GWs

<sup>5</sup> More discussion on the bubble wall velocity in “runaway” case see e.g. [151].

from these three processes can be found in the literature [152, 166, 174, 176, 177]. The total GWs signal is the linear superposition of these three:

$$h^2\Omega_{\text{GW}}(f) = h^2\Omega_b(f) + h^2\Omega_s(f) + h^2\Omega_t(f). \quad (46)$$

Each term on the right hand side of above equation can be decomposed into peak amplitudes ( $\Omega_{b,s,t}^{\text{peak}}$ ) and spectral shape functions ( $\mathcal{S}_{b,s,t}$ ):

$$\begin{aligned} h^2\Omega_b(f) &\simeq h^2\Omega_b^{\text{peak}} \mathcal{S}_b(f, f_b^{\text{peak}}), \\ h^2\Omega_s(f) &\simeq h^2\Omega_s^{\text{peak}} \mathcal{S}_s(f, f_s^{\text{peak}}), \\ h^2\Omega_t(f) &\simeq h^2\Omega_t^{\text{peak}} \mathcal{S}_t(f, f_t^{\text{peak}}), \end{aligned} \quad (47)$$

where the peak amplitudes are determined by

$$\begin{aligned} h^2\Omega_b^{\text{peak}} &= 1.24 \times 10^{-5} \left(\frac{h_{\text{eff}0}}{h_{\text{eff}*}}\right)^{4/3} (g_{\text{eff}*})(\xi_\infty)^4 \left(\frac{0.11v_w}{0.42 + v_w^2}\right) \left(\frac{\kappa_b \mathbb{A}}{1 + \mathbb{A}}\right)^2 \left(\frac{v_w}{\beta/H_*}\right)^2, \\ h^2\Omega_s^{\text{peak}} &= 1.97 \times 10^{-6} \left(\frac{h_{\text{eff}0}}{h_{\text{eff}*}}\right)^{4/3} (g_{\text{eff}*})(\xi_\infty)^4 \left(\frac{\kappa_s \mathbb{A}}{1 + \mathbb{A}}\right)^2 \left(\frac{v_w}{\beta/H_*}\right), \\ h^2\Omega_t^{\text{peak}} &= 2.49 \times 10^{-4} \left(\frac{h_{\text{eff}0}}{h_{\text{eff}*}}\right)^{4/3} (g_{\text{eff}*})(\xi_\infty)^4 \left(\frac{\kappa_t \mathbb{A}}{1 + \mathbb{A}}\right)^{3/2} \left(\frac{v_w}{\beta/H_*}\right), \end{aligned} \quad (48)$$

Here  $h_{\text{eff}}$  and  $g_{\text{eff}}$  indicate the total effective d.o.f. for entropy and energy respectively <sup>6</sup>, and “0” corresponds to current time. The spectral shape functions are given by:

$$\begin{aligned} \mathcal{S}_b(f, f_b^{\text{peak}}) &= \left(\frac{f}{f_b^{\text{peak}}}\right)^{2.8} \left[ \frac{3.8}{1 + 2.8(f/f_b^{\text{peak}})^{3.8}} \right], \\ \mathcal{S}_s(f, f_s^{\text{peak}}) &= \left(\frac{f}{f_s^{\text{peak}}}\right)^3 \left[ \frac{7}{4 + 3(f/f_s^{\text{peak}})^2} \right]^{7/2}, \\ \mathcal{S}_t(f, f_t^{\text{peak}}) &= \left(\frac{f}{f_t^{\text{peak}}}\right)^3 \left[ \frac{1}{1 + (f/f_t^{\text{peak}})} \right]^{11/3} \frac{1}{1 + 8\pi f/h_*}, \end{aligned} \quad (49)$$

with

$$h_* = \frac{a_*}{a_0} H_* = 7.44 \times 10^{-11} \text{Hz} \left(\frac{g_{\text{eff}*}^{1/2}}{h_{\text{eff}*}^{1/3}}\right) \left(\frac{h_{\text{eff}0}}{3.91}\right)^{1/3} \xi_\infty \left(\frac{T_*}{1 \text{ MeV}}\right). \quad (50)$$

The peak frequencies in shape functions are given by:

$$f_b^{\text{peak}} = 7.44 \times 10^{-11} \text{Hz} \left(\frac{g_{\text{eff}*}^{1/2}}{h_{\text{eff}*}^{1/3}}\right) \left(\frac{h_{\text{eff}0}}{3.91}\right)^{1/3} \xi_\infty \left(\frac{T_*}{1 \text{ MeV}}\right) \left(\frac{\beta/H_*}{v_w}\right) \left(\frac{0.62v_w}{1.8 - 0.1v_w + v_w^2}\right), \quad (51)$$

---

<sup>6</sup> It should be noticed that the definition of  $h_{\text{eff}}$  and  $g_{\text{eff}}$  is the same as our previous work [42], i.e. we let the total radiation energy density and entropy density to be proportional to the fourth and third powers of the dark sector temperature, respectively.

$$f_s^{\text{peak}} = 8.59 \times 10^{-11} \text{Hz} \left( \frac{g_{\text{eff}*}^{1/2}}{h_{\text{eff}*}^{1/3}} \right) \left( \frac{h_{\text{eff}0}}{3.91} \right)^{1/3} \xi_\infty \left( \frac{T_*}{1 \text{ MeV}} \right) \left( \frac{\beta/H_*}{v_w} \right), \quad (52)$$

$$f_t^{\text{peak}} = 13.0 \times 10^{-11} \text{Hz} \left( \frac{g_{\text{eff}*}^{1/2}}{h_{\text{eff}*}^{1/3}} \right) \left( \frac{h_{\text{eff}0}}{3.91} \right)^{1/3} \xi_\infty \left( \frac{T_*}{1 \text{ MeV}} \right) \left( \frac{\beta/H_*}{v_w} \right). \quad (53)$$

#### IV PARAMETER SPACE SCAN RESULTS

In this section we present a parameter space scan. There are 5 input parameters in this work, i.e.  $\{ m_\chi, m_{A'}, \alpha', m_s, \xi_{\text{reh}} \}$ . Their ranges are:

$$10 \text{ GeV} < m_\chi < 600 \text{ GeV}, \quad 0.1 \text{ MeV} < m_{A'} < 10 \text{ MeV}, \quad 0.005 < \alpha' < 0.4 \quad (54)$$

$$\sqrt{\frac{\alpha' m_{A'}^2}{3\pi}} < m_s < \frac{1}{2} m_{A'}, \quad 0.1 < \xi_{\text{reh}} < 2.0 \quad (55)$$

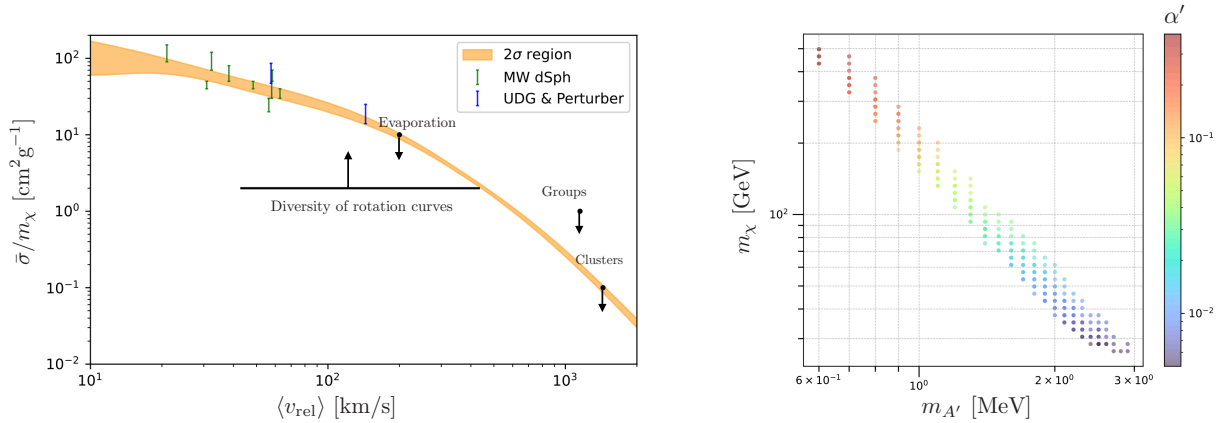


FIG. 2. Left:  $\bar{\sigma}/m_\chi$  as function of average DM relative velocity  $\langle v_{\text{rel}} \rangle$ . Small-scale data and limits are also shown. Orange region corresponds to  $2\sigma$  region. Right: the parameter space composed by  $\{ m_\chi, m_{A'}, \alpha' \}$  which is within the  $2\sigma$  region.

The first restriction we impose on the parameter space is that the velocity-dependent DM scattering cross section  $\bar{\sigma}$  given by a parameter point is within the  $2\sigma$  confidence interval obtained from small-scale data, as we explained in Sec. III A. In Fig. 2 we present the scan results, which shows that the small-scale data and limits compress the parameter sub-space composed by  $\{ m_\chi, m_{A'}, \alpha' \}$  into a quite small region.

The parameter points which is consistent with small-scale data are used for further analysis. In Fig. 3 we present the peak amplitudes of GWs (labeled as  $h^2 \Omega_{\text{GW}}^{\text{peak}}$ ),  $\Delta N_{\text{eff}}$ , and DR-DM interaction strength parameter  $a_{\text{dark}}$  calculated from those parameter points. We find that  $h^2 \Omega_{\text{GW}}^{\text{peak}}$  is mainly

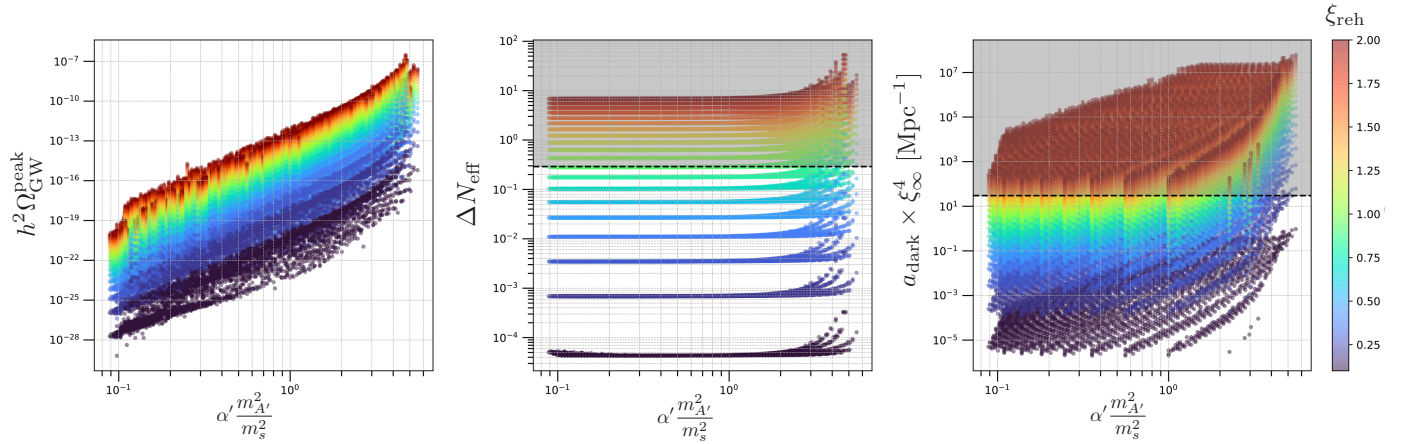


FIG. 3. The samples consistent with the small-scale data. Left: peak amplitudes of GWs as functions of parameter combination  $\alpha' \frac{m_{A'}^2}{m_s^2}$ , with color-mapped by initial temperature ratio  $\xi_{\text{reh}}$ . Middle:  $\Delta N_{\text{eff}}$  as functions of parameter combination  $\alpha' \frac{m_{A'}^2}{m_s^2}$ , with color-mapped by initial temperature ratio  $\xi_{\text{reh}}$ . Gray region has been excluded by current data. Right:  $a_{\text{dark}} \times \xi_{\infty}^4$  as functions of parameter combination  $\alpha' \frac{m_{A'}^2}{m_s^2}$ , with color-mapped by initial temperature ratio  $\xi_{\text{reh}}$ . Gray region has been excluded by current data.

determined by parameter combination  $\alpha' \frac{m_{A'}^2}{m_s^2}$  and initial temperature ratio  $\xi_{\text{reh}}$ . Generally speaking,  $\alpha' \frac{m_{A'}^2}{m_s^2}$  controls the strength of FOPT and  $\xi_{\text{reh}}$  roughly determines the energy density in the dark sector. Without considering other limits, in Fig. 3 (Left) we see that  $h^2 \Omega_{\text{GW}}^{\text{peak}}$  can be large as  $10^{-7}$ , which is promising to be detected by future GWs detectors like SKA telescope [178] or space-based LISA interferometer [179], provided the peak frequency is not far from the sensitive regions of SKA or LISA. However, as presented in Fig. 3 (Middle, Right)  $\Delta N_{\text{eff}}$  and DR-DM interaction put very strong bounds on the parameter space, and thus limit the available value of  $h^2 \Omega_{\text{GW}}^{\text{peak}}$ .

To further illuminate the impact from  $\Delta N_{\text{eff}}$  and DR-DM interaction, we present Fig. 4 which clearly show how  $h^2 \Omega_{\text{GW}}^{\text{peak}}$  are constrained by bounds. The maxima of  $h^2 \Omega_{\text{GW}}^{\text{peak}}$  is suppressed by more than 4-orders when considering these two bounds.

In Fig. 5 we further project parameter points on the standard “frequency-amplitude” plane, with the “powerlaw-integrated sensitivity curves” (PLISCs) of SKA and LISA also presented [153, 180]. The PLISC of SKA is normalized to “observing time = 20 years” and “signal-to-noise ratio = 1”, while the PLISC of LISA is normalized to “observing time = 1 year” and “signal-to-noise ratio = 1”. If the GWs spectrum from a parameter point intersect with a PLISC, then this parameter point can be treated as detectable at the corresponding experiment. To avoid clutter in the image, we only depict the peaks of GWs spectrum in Fig. 5 instead of showing the complete spectrum. In Fig. 5 (Left) we see that without considering current  $\Delta N_{\text{eff}}$  and Lyman- $\alpha$  constraints, a considerable number of parameter points can be detected by SKA. However, Fig. 5 (Right) shows that, taking both constraints into account, all the

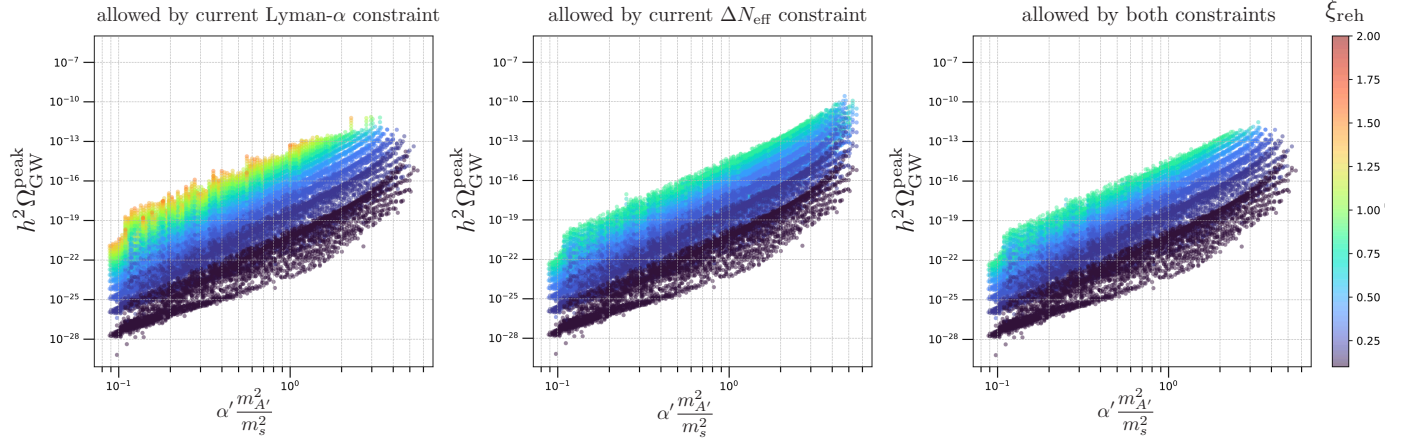


FIG. 4. The samples consistent with the small-scale data. Left: parameter points allowed by current Lyman- $\alpha$  constraint. Middle: parameter points allowed by current  $\Delta N_{\text{eff}}$  constraint. Right: parameter points allowed by both constraints.

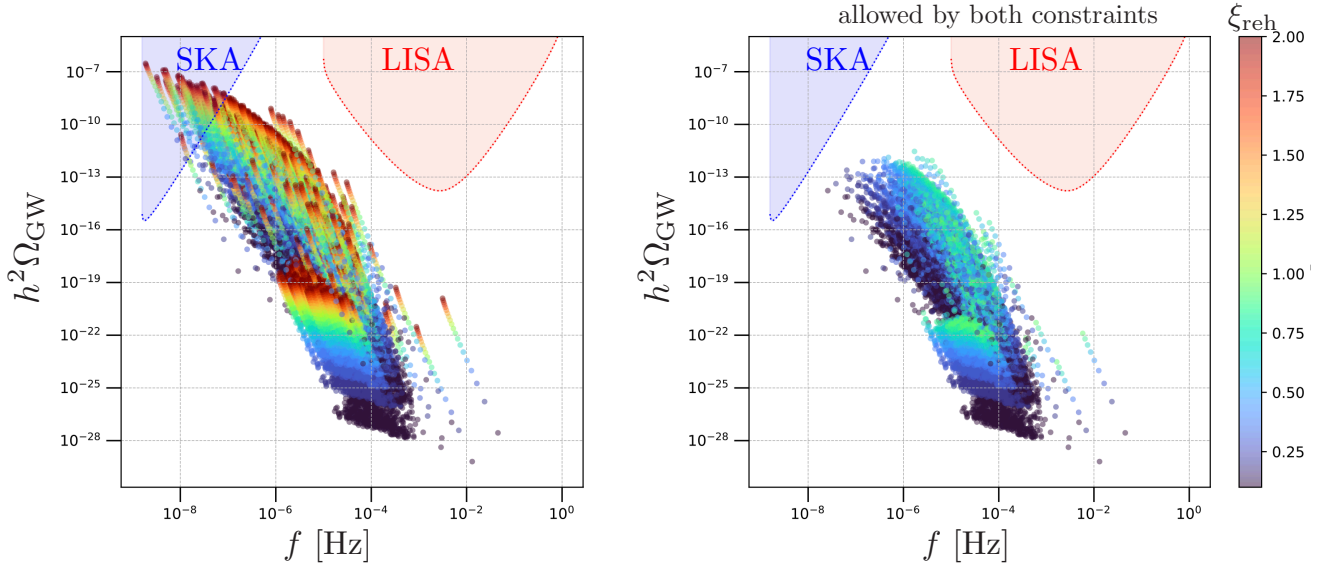


FIG. 5. The samples consistent with the small-scale data. The blue dotted line and red dotted line are PLISC of SKA and LISA, respectively. Left: the current  $\Delta N_{\text{eff}}$  and Lyman- $\alpha$  constraints are not considered. Right: both constraints are considered.

peaks are below the PLISC of SKA. We have checked numerically that not only the peaks of these parameter points are not inside the PLISC, but their entire spectrums also do not intersect with the PLISC. So the conclusion we draw here is that, considering current  $\Delta N_{\text{eff}}$  and Lyman- $\alpha$  constraints, we cannot detect the secluded self-interacting dark sector discussed in this paper through future GWs

detection experiments such as SKA and LISA.

## V CONCLUSION

In this work we studied the detection of the gravitational waves generated by a secluded dark sector. The portal between the dark sector and the visible sector is turned off and thus the entropy of each sector is separately conserved. The dark sector is charged under a dark  $U(1)'$  which is spontaneously broken. The dark matter self-interaction induced by this dark  $U(1)'$  can be consistent with the small-scale structure observations. Furthermore, the symmetry breaking process of this dark  $U(1)'$ , which can be a first-order phase transition, might generate detectable gravitational wave signals. Whereas, this secluded dark sector is constrained by the  $\Delta N_{\text{eff}}$  measurement and the Lyman- $\alpha$  observation. Through a parameter space scan, we found that the combined constraints make this model unable to generate any gravitational waves accessible at SKA or LISA.

However, so far we should still keep an open mind for the possibility to detect the gravitational waves generated by such a dark sector. The main reason is that the current theoretical calculation method for the gravitational waves might have sizable theoretical uncertainties. To significantly reduce or reasonably estimate the theoretical uncertainties is crucial, which leaves in our future work.

## ACKNOWLEDGEMENTS

M. Z. appreciates helpful discussions with Yue-Lin Sming Tsai and Chi Zhang. This work was supported by the Natural Science Foundation of China (NSFC) under Grants Nos. 12105118, 11947118 and 12335005, by the Research Fund for Outstanding Talents (Grant No. 5101029470335) from Henan Normal University, and by the Peng-Huan-Wu Theoretical Physics Innovation Center (Grant No. 12047503) funded by the National Natural Science Foundation of China.

- 
- [1] Douglas Clowe, Marusa Bradac, Anthony H. Gonzalez, Maxim Markevitch, Scott W. Randall, Christine Jones, and Dennis Zaritsky, “A direct empirical proof of the existence of dark matter,” *Astrophys. J. Lett.* **648**, L109–L113 (2006), [arXiv:astro-ph/0608407](#).
  - [2] N. Aghanim *et al.* (Planck), “Planck 2018 results. VI. Cosmological parameters,” *Astron. Astrophys.* **641**, A6 (2020), [Erratum: *Astron. Astrophys.* 652, C4 (2021)], [arXiv:1807.06209 \[astro-ph.CO\]](#).
  - [3] George R. Blumenthal, S. M. Faber, Joel R. Primack, and Martin J. Rees, “Formation of Galaxies and Large Scale Structure with Cold Dark Matter,” *Nature* **311**, 517–525 (1984).
  - [4] Volker Springel, Carlos S. Frenk, and Simon D. M. White, “The large-scale structure of the Universe,” *Nature* **440**, 1137 (2006), [arXiv:astro-ph/0604561](#).

- [5] Ben Moore, Thomas R. Quinn, Fabio Governato, Joachim Stadel, and George Lake, “Cold collapse and the core catastrophe,” *Mon. Not. Roy. Astron. Soc.* **310**, 1147–1152 (1999), [arXiv:astro-ph/9903164](#).
- [6] B. Moore, “Evidence against dissipationless dark matter from observations of galaxy haloes,” *Nature* **370**, 629 (1994).
- [7] Ricardo A. Flores and Joel R. Primack, “Observational and theoretical constraints on singular dark matter halos,” *Astrophys. J. Lett.* **427**, L1–4 (1994), [arXiv:astro-ph/9402004](#).
- [8] Kyle A. Oman *et al.*, “The unexpected diversity of dwarf galaxy rotation curves,” *Mon. Not. Roy. Astron. Soc.* **452**, 3650–3665 (2015), [arXiv:1504.01437 \[astro-ph.GA\]](#).
- [9] B. Moore, S. Ghigna, F. Governato, G. Lake, Thomas R. Quinn, J. Stadel, and P. Tozzi, “Dark matter substructure within galactic halos,” *Astrophys. J. Lett.* **524**, L19–L22 (1999), [arXiv:astro-ph/9907411](#).
- [10] Anatoly A. Klypin, Andrey V. Kravtsov, Octavio Valenzuela, and Francisco Prada, “Where are the missing Galactic satellites?” *Astrophys. J.* **522**, 82–92 (1999), [arXiv:astro-ph/9901240](#).
- [11] Michael Boylan-Kolchin, James S. Bullock, and Manoj Kaplinghat, “The Milky Way’s bright satellites as an apparent failure of LCDM,” *Mon. Not. Roy. Astron. Soc.* **422**, 1203–1218 (2012), [arXiv:1111.2048 \[astro-ph.CO\]](#).
- [12] Michael Boylan-Kolchin, James S. Bullock, and Manoj Kaplinghat, “Too big to fail? The puzzling darkness of massive Milky Way subhaloes,” *Mon. Not. Roy. Astron. Soc.* **415**, L40 (2011), [arXiv:1103.0007 \[astro-ph.CO\]](#).
- [13] C. S. Kochanek and Martin J. White, “A Quantitative study of interacting dark matter in halos,” *Astrophys. J.* **543**, 514 (2000), [arXiv:astro-ph/0003483](#).
- [14] Kevin E. Andrade, Jackson Fuson, Sophia Gad-Nasr, Demao Kong, Quinn Minor, M. Grant Roberts, and Manoj Kaplinghat, “A stringent upper limit on dark matter self-interaction cross-section from cluster strong lensing,” *Mon. Not. Roy. Astron. Soc.* **510**, 54–81 (2021), [arXiv:2012.06611 \[astro-ph.CO\]](#).
- [15] Oliver D. Elbert, James S. Bullock, Manoj Kaplinghat, Shea Garrison-Kimmel, Andrew S. Graus, and Miguel Rocha, “A Testable Conspiracy: Simulating Baryonic Effects on Self-Interacting Dark Matter Halos,” *Astrophys. J.* **853**, 109 (2018), [arXiv:1609.08626 \[astro-ph.GA\]](#).
- [16] A. Bastidas Fry, F. Governato, A. Pontzen, T. Quinn, M. Tremmel, L. Anderson, H. Menon, A. M. Brooks, and J. Wadsley, “All about baryons: revisiting SIDM predictions at small halo masses,” *Mon. Not. Roy. Astron. Soc.* **452**, 1468–1479 (2015), [arXiv:1501.00497 \[astro-ph.CO\]](#).
- [17] Naoki Yoshida, Volker Springel, Simon D. M. White, and Giuseppe Tormen, “Collisional dark matter and the structure of dark halos,” *Astrophys. J. Lett.* **535**, L103 (2000), [arXiv:astro-ph/0002362](#).
- [18] Ben Moore, Sergio Gelato, Adrian Jenkins, F. R. Pearce, and Vicent Quilis, “Collisional versus collisionless dark matter,” *Astrophys. J. Lett.* **535**, L21–L24 (2000), [arXiv:astro-ph/0002308](#).
- [19] Jesus Zavala, Mark Vogelsberger, and Matthew G. Walker, “Constraining Self-Interacting Dark Matter with the Milky Way’s dwarf spheroidals,” *Mon. Not. Roy. Astron. Soc.* **431**, L20–L24 (2013), [arXiv:1211.6426 \[astro-ph.CO\]](#).
- [20] Oliver D. Elbert, James S. Bullock, Shea Garrison-Kimmel, Miguel Rocha, Jose Oñorbe, and Annika H. G. Peter, “Core formation in dwarf haloes with self-interacting dark matter: no fine-tuning necessary,” *Mon. Not. Roy. Astron. Soc.* **453**, 29–37 (2015), [arXiv:1412.1477 \[astro-ph.GA\]](#).
- [21] Miguel Rocha, Annika H. G. Peter, James S. Bullock, Manoj Kaplinghat, Shea Garrison-Kimmel, Jose Onorbe, and Leonidas A. Moustakas, “Cosmological Simulations with Self-Interacting Dark Matter I: Constant Density Cores and Substructure,” *Mon. Not. Roy. Astron. Soc.* **430**, 81–104 (2013), [arXiv:1208.3025](#)

- [astro-ph.CO].
- [22] Annika H. G. Peter, Miguel Rocha, James S. Bullock, and Manoj Kaplinghat, “Cosmological Simulations with Self-Interacting Dark Matter II: Halo Shapes vs. Observations,” *Mon. Not. Roy. Astron. Soc.* **430**, 105 (2013), arXiv:1208.3026 [astro-ph.CO].
- [23] Manoj Kaplinghat, Sean Tulin, and Hai-Bo Yu, “Dark Matter Halos as Particle Colliders: Unified Solution to Small-Scale Structure Puzzles from Dwarfs to Clusters,” *Phys. Rev. Lett.* **116**, 041302 (2016), arXiv:1508.03339 [astro-ph.CO].
- [24] Sean Tulin and Hai-Bo Yu, “Dark Matter Self-interactions and Small Scale Structure,” *Phys. Rept.* **730**, 1–57 (2018), arXiv:1705.02358 [hep-ph].
- [25] Mark Vogelsberger, Jesus Zavala, Christine Simpson, and Adrian Jenkins, “Dwarf galaxies in CDM and SIDM with baryons: observational probes of the nature of dark matter,” *Mon. Not. Roy. Astron. Soc.* **444**, 3684–3698 (2014), arXiv:1405.5216 [astro-ph.CO].
- [26] Gregory A. Dooley, Annika H. G. Peter, Mark Vogelsberger, Jesús Zavala, and Anna Frebel, “Enhanced Tidal Stripping of Satellites in the Galactic Halo from Dark Matter Self-Interactions,” *Mon. Not. Roy. Astron. Soc.* **461**, 710–727 (2016), arXiv:1603.08919 [astro-ph.GA].
- [27] Romeel Dave, David N. Spergel, Paul J. Steinhardt, and Benjamin D. Wandelt, “Halo properties in cosmological simulations of selfinteracting cold dark matter,” *Astrophys. J.* **547**, 574–589 (2001), arXiv:astro-ph/0006218.
- [28] Andrew Robertson, David Harvey, Richard Massey, Vincent Eke, Ian G. McCarthy, Mathilde Jauzac, Baojiu Li, and Joop Schaye, “Observable tests of self-interacting dark matter in galaxy clusters: cosmological simulations with SIDM and baryons,” *Mon. Not. Roy. Astron. Soc.* **488**, 3646–3662 (2019), arXiv:1810.05649 [astro-ph.CO].
- [29] David N. Spergel and Paul J. Steinhardt, “Observational evidence for selfinteracting cold dark matter,” *Phys. Rev. Lett.* **84**, 3760–3763 (2000), arXiv:astro-ph/9909386.
- [30] Pedro Colin, Vladimir Avila-Reese, Octavio Valenzuela, and Claudio Firmani, “Structure and subhalo population of halos in a selfinteracting dark matter cosmology,” *Astrophys. J.* **581**, 777–793 (2002), arXiv:astro-ph/0205322.
- [31] Mark Vogelsberger, Jesus Zavala, and Abraham Loeb, “Subhaloes in Self-Interacting Galactic Dark Matter Haloes,” *Mon. Not. Roy. Astron. Soc.* **423**, 3740 (2012), arXiv:1201.5892 [astro-ph.CO].
- [32] David Harvey, Richard Massey, Thomas Kitching, Andy Taylor, and Eric Tittley, “The non-gravitational interactions of dark matter in colliding galaxy clusters,” *Science* **347**, 1462–1465 (2015), arXiv:1503.07675 [astro-ph.CO].
- [33] Andreas Burkert, “The Structure and evolution of weakly selfinteracting cold dark matter halos,” *Astrophys. J. Lett.* **534**, L143–L146 (2000), arXiv:astro-ph/0002409.
- [34] Laura Sagunski, Sophia Gad-Nasr, Brian Colquhoun, Andrew Robertson, and Sean Tulin, “Velocity-dependent Self-interacting Dark Matter from Groups and Clusters of Galaxies,” *JCAP* **01**, 024 (2021), arXiv:2006.12515 [astro-ph.CO].
- [35] Naoki Yoshida, Volker Springel, Simon D. M. White, and Giuseppe Tormen, “Weakly self-interacting dark matter and the structure of dark halos,” *Astrophys. J. Lett.* **544**, L87–L90 (2000), arXiv:astro-ph/0006134.
- [36] Daneng Yang, Ethan O. Nadler, and Hai-Bo Yu, “Strong Dark Matter Self-interactions Diversify Halo Populations within and surrounding the Milky Way,” *Astrophys. J.* **949**, 67 (2023), arXiv:2211.13768 [astro-ph.GA].

- [37] Amin Aboubrabim, Wan-Zhe Feng, Pran Nath, and Zhu-Yao Wang, “Self-interacting hidden sector dark matter, small scale galaxy structure anomalies, and a dark force,” *Phys. Rev. D* **103**, 075014 (2021), [arXiv:2008.00529 \[hep-ph\]](#).
- [38] Brando Bellazzini, Mathieu Cliche, and Philip Tanedo, “Effective theory of self-interacting dark matter,” *Phys. Rev. D* **88**, 083506 (2013), [arXiv:1307.1129 \[hep-ph\]](#).
- [39] Kimberly K. Boddy, Jonathan L. Feng, Manoj Kaplinghat, Yael Shadmi, and Timothy M. P. Tait, “Strongly interacting dark matter: Self-interactions and keV lines,” *Phys. Rev. D* **90**, 095016 (2014), [arXiv:1408.6532 \[hep-ph\]](#).
- [40] Torsten Bringmann, Jasper Hasenkamp, and Jörn Kersten, “Tight bonds between sterile neutrinos and dark matter,” *JCAP* **07**, 042 (2014), [arXiv:1312.4947 \[hep-ph\]](#).
- [41] Matthew R. Buckley and Patrick J. Fox, “Dark Matter Self-Interactions and Light Force Carriers,” *Phys. Rev. D* **81**, 083522 (2010), [arXiv:0911.3898 \[hep-ph\]](#).
- [42] Zien Chen, Kairui Ye, and Mengchao Zhang, “Asymmetric dark matter with a spontaneously broken  $U(1)'$ : Self-interaction and gravitational waves,” *Phys. Rev. D* **107**, 095027 (2023), [arXiv:2303.11820 \[hep-ph\]](#).
- [43] Michael Duerr, Kai Schmidt-Hoberg, and Sebastian Wild, “Self-interacting dark matter with a stable vector mediator,” *JCAP* **09**, 033 (2018), [arXiv:1804.10385 \[hep-ph\]](#).
- [44] Jonathan L. Feng, Manoj Kaplinghat, and Hai-Bo Yu, “Halo Shape and Relic Density Exclusions of Sommerfeld-Enhanced Dark Matter Explanations of Cosmic Ray Excesses,” *Phys. Rev. Lett.* **104**, 151301 (2010), [arXiv:0911.0422 \[hep-ph\]](#).
- [45] Jonathan L. Feng, Manoj Kaplinghat, Huitzu Tu, and Hai-Bo Yu, “Hidden Charged Dark Matter,” *JCAP* **07**, 004 (2009), [arXiv:0905.3039 \[hep-ph\]](#).
- [46] R. Foot and S. Vagnozzi, “Diurnal modulation signal from dissipative hidden sector dark matter,” *Phys. Lett. B* **748**, 61–66 (2015), [arXiv:1412.0762 \[hep-ph\]](#).
- [47] R. Foot and S. Vagnozzi, “Dissipative hidden sector dark matter,” *Phys. Rev. D* **91**, 023512 (2015), [arXiv:1409.7174 \[hep-ph\]](#).
- [48] Robert Foot and Sunny Vagnozzi, “Solving the small-scale structure puzzles with dissipative dark matter,” *JCAP* **07**, 013 (2016), [arXiv:1602.02467 \[astro-ph.CO\]](#).
- [49] Kimmo Kainulainen, Kimmo Tuominen, and Ville Vaskonen, “Self-interacting dark matter and cosmology of a light scalar mediator,” *Phys. Rev. D* **93**, 015016 (2016), [Erratum: *Phys.Rev.D* 95, 079901 (2017)], [arXiv:1507.04931 \[hep-ph\]](#).
- [50] Ayuki Kamada, Masaki Yamada, and Tsutomu T. Yanagida, “Self-interacting dark matter with a vector mediator: kinetic mixing with the  $U(1)_{(B-L)_3}$  gauge boson,” *JHEP* **03**, 021 (2019), [arXiv:1811.02567 \[hep-ph\]](#).
- [51] Ayuki Kamada, Kunio Kaneta, Keisuke Yanagi, and Hai-Bo Yu, “Self-interacting dark matter and muon  $g - 2$  in a gauged  $U(1)_{L_\mu - L_\tau}$  model,” *JHEP* **06**, 117 (2018), [arXiv:1805.00651 \[hep-ph\]](#).
- [52] Ayuki Kamada, Masaki Yamada, and Tsutomu T. Yanagida, “Unification of the standard model and dark matter sectors in  $[SU(5) \times U(1)]^4$ ,” *JHEP* **07**, 180 (2019), [arXiv:1905.04245 \[hep-ph\]](#).
- [53] Ayuki Kamada, Masaki Yamada, and Tsutomu T. Yanagida, “Unification for darkly charged dark matter,” *Phys. Rev. D* **102**, 015012 (2020), [arXiv:1908.00207 \[hep-ph\]](#).
- [54] Ayuki Kamada, Hee Jung Kim, and Takumi Kuwahara, “Maximally self-interacting dark matter: models and predictions,” *JHEP* **12**, 202 (2020), [arXiv:2007.15522 \[hep-ph\]](#).

- [55] Zhaofeng Kang, “View FImP miracle (by scale invariance) à la self-interaction,” *Phys. Lett. B* **751**, 201–204 (2015), [arXiv:1505.06554 \[hep-ph\]](#).
- [56] Teppei Kitahara and Yasuhiro Yamamoto, “Protophobic Light Vector Boson as a Mediator to the Dark Sector,” *Phys. Rev. D* **95**, 015008 (2017), [arXiv:1609.01605 \[hep-ph\]](#).
- [57] P. Ko and Yong Tang, “ $\nu$ AMDM: A model for sterile neutrino and dark matter reconciles cosmological and neutrino oscillation data after BICEP2,” *Phys. Lett. B* **739**, 62–67 (2014), [arXiv:1404.0236 \[hep-ph\]](#).
- [58] P. Ko and Y. Tang, “Self-interacting scalar dark matter with local  $Z_3$  symmetry,” *JCAP* **05**, 047 (2014), [arXiv:1402.6449 \[hep-ph\]](#).
- [59] Abraham Loeb and Neal Weiner, “Cores in Dwarf Galaxies from Dark Matter with a Yukawa Potential,” *Phys. Rev. Lett.* **106**, 171302 (2011), [arXiv:1011.6374 \[astro-ph.CO\]](#).
- [60] Ernest Ma, “Inception of Self-Interacting Dark Matter with Dark Charge Conjugation Symmetry,” *Phys. Lett. B* **772**, 442–445 (2017), [arXiv:1704.04666 \[hep-ph\]](#).
- [61] Katelin Schutz and Tracy R. Slatyer, “Self-Scattering for Dark Matter with an Excited State,” *JCAP* **01**, 021 (2015), [arXiv:1409.2867 \[hep-ph\]](#).
- [62] Sean Tulin, Hai-Bo Yu, and Kathryn M. Zurek, “Resonant Dark Forces and Small Scale Structure,” *Phys. Rev. Lett.* **110**, 111301 (2013), [arXiv:1210.0900 \[hep-ph\]](#).
- [63] Sean Tulin, Hai-Bo Yu, and Kathryn M. Zurek, “Beyond Collisionless Dark Matter: Particle Physics Dynamics for Dark Matter Halo Structure,” *Phys. Rev. D* **87**, 115007 (2013), [arXiv:1302.3898 \[hep-ph\]](#).
- [64] Laura G. van den Aarssen, Torsten Bringmann, and Christoph Pfrommer, “Is dark matter with long-range interactions a solution to all small-scale problems of  $\Lambda$ CDM cosmology?” *Phys. Rev. Lett.* **109**, 231301 (2012), [arXiv:1205.5809 \[astro-ph.CO\]](#).
- [65] Wenyu Wang, Mengchao Zhang, and Jun Zhao, “Higgs exotic decays in general NMSSM with self-interacting dark matter,” *Int. J. Mod. Phys. A* **33**, 1841002 (2018), [arXiv:1604.00123 \[hep-ph\]](#).
- [66] Paul Frederik Depta, Marco Hufnagel, and Kai Schmidt-Hoberg, “Updated BBN constraints on electromagnetic decays of MeV-scale particles,” *JCAP* **04**, 011 (2021), [arXiv:2011.06519 \[hep-ph\]](#).
- [67] Marco Hufnagel, Kai Schmidt-Hoberg, and Sebastian Wild, “BBN constraints on MeV-scale dark sectors. Part II. Electromagnetic decays,” *JCAP* **11**, 032 (2018), [arXiv:1808.09324 \[hep-ph\]](#).
- [68] Masahiro Ibe, Shin Kobayashi, Yuhei Nakayama, and Satoshi Shirai, “Cosmological constraints on dark scalar,” *JHEP* **03**, 198 (2022), [arXiv:2112.11096 \[hep-ph\]](#).
- [69] Jae Hyeok Chang, Rouven Essig, and Samuel D. McDermott, “Revisiting Supernova 1987A Constraints on Dark Photons,” *JHEP* **01**, 107 (2017), [arXiv:1611.03864 \[hep-ph\]](#).
- [70] Eugenio Del Nobile, Manoj Kaplinghat, and Hai-Bo Yu, “Direct Detection Signatures of Self-Interacting Dark Matter with a Light Mediator,” *JCAP* **10**, 055 (2015), [arXiv:1507.04007 \[hep-ph\]](#).
- [71] Stefania Gori, Gilad Perez, and Kohsaku Tobioka, “KOTO vs. NA62 Dark Scalar Searches,” *JHEP* **08**, 110 (2020), [arXiv:2005.05170 \[hep-ph\]](#).
- [72] Mattias Blennow, Enrique Fernandez-Martinez, Olga Mena, Javier Redondo, and Paolo Serra, “Asymmetric Dark Matter and Dark Radiation,” *JCAP* **07**, 022 (2012), [arXiv:1203.5803 \[hep-ph\]](#).
- [73] Andrea Addazi and Antonino Marciano, “Gravitational waves from dark first order phase transitions and dark photons,” *Chin. Phys. C* **42**, 023107 (2018), [arXiv:1703.03248 \[hep-ph\]](#).
- [74] Andrea Addazi, Yi-Fu Cai, Qingyu Gan, Antonino Marciano, and Kaiqiang Zeng, “NANOGrav results and dark first order phase transitions,” *Sci. China Phys. Mech. Astron.* **64**, 290411 (2021), [arXiv:2009.10327 \[hep-ph\]](#).

- [75] Aleksandr Azatov, Miguel Vanvlasselaer, and Wen Yin, “Dark Matter production from relativistic bubble walls,” *JHEP* **03**, 288 (2021), [arXiv:2101.05721 \[hep-ph\]](#).
- [76] Aleksandr Azatov, Giulio Barni, Sabyasachi Chakraborty, Miguel Vanvlasselaer, and Wen Yin, “Ultra-relativistic bubbles from the simplest Higgs portal and their cosmological consequences,” *JHEP* **10**, 017 (2022), [arXiv:2207.02230 \[hep-ph\]](#).
- [77] Yang Bai, Andrew J. Long, and Sida Lu, “Dark Quark Nuggets,” *Phys. Rev. D* **99**, 055047 (2019), [arXiv:1810.04360 \[hep-ph\]](#).
- [78] Moritz Breitbach, Joachim Kopp, Eric Madge, Toby Opferkuch, and Pedro Schwaller, “Dark, Cold, and Noisy: Constraining Secluded Hidden Sectors with Gravitational Waves,” *JCAP* **07**, 007 (2019), [arXiv:1811.11175 \[hep-ph\]](#).
- [79] Francesco Costa, Sarif Khan, and Jinsu Kim, “A two-component vector WIMP — fermion FIMP dark matter model with an extended seesaw mechanism,” *JHEP* **12**, 165 (2022), [arXiv:2209.13653 \[hep-ph\]](#).
- [80] Francesco Costa, Sarif Khan, and Jinsu Kim, “A two-component dark matter model and its associated gravitational waves,” *JHEP* **06**, 026 (2022), [arXiv:2202.13126 \[hep-ph\]](#).
- [81] James B. Dent, Bhaskar Dutta, Sumit Ghosh, Jason Kumar, and Jack Runburg, “Sensitivity to dark sector scales from gravitational wave signatures,” *JHEP* **08**, 300 (2022), [arXiv:2203.11736 \[hep-ph\]](#).
- [82] Malcolm Fairbairn, Edward Hardy, and Alastair Wickens, “Hearing without seeing: gravitational waves from hot and cold hidden sectors,” *JHEP* **07**, 044 (2019), [arXiv:1901.11038 \[hep-ph\]](#).
- [83] Tathagata Ghosh, Huai-Ke Guo, Tao Han, and Hongkai Liu, “Electroweak phase transition with an SU(2) dark sector,” *JHEP* **07**, 045 (2021), [arXiv:2012.09758 \[hep-ph\]](#).
- [84] Chengcheng Han, Ke-Pan Xie, Jin Min Yang, and Mengchao Zhang, “Self-interacting dark matter implied by nano-Hertz gravitational waves,” *Phys. Rev. D* **109**, 115025 (2024), [arXiv:2306.16966 \[hep-ph\]](#).
- [85] Katsuya Hashino, Mitsuru Kakizaki, Shinya Kanemura, Pyungwon Ko, and Toshinori Matsui, “Gravitational waves from first order electroweak phase transition in models with the  $U(1)_X$  gauge symmetry,” *JHEP* **06**, 088 (2018), [arXiv:1802.02947 \[hep-ph\]](#).
- [86] Fa Peng Huang and Jiang-Hao Yu, “Exploring inert dark matter blind spots with gravitational wave signatures,” *Phys. Rev. D* **98**, 095022 (2018), [arXiv:1704.04201 \[hep-ph\]](#).
- [87] Joerg Jaeckel, Valentin V. Khoze, and Michael Spannowsky, “Hearing the signal of dark sectors with gravitational wave detectors,” *Phys. Rev. D* **94**, 103519 (2016), [arXiv:1602.03901 \[hep-ph\]](#).
- [88] Wolfram Ratzinger and Pedro Schwaller, “Whispers from the dark side: Confronting light new physics with NANOGrav data,” *SciPost Phys.* **10**, 047 (2021), [arXiv:2009.11875 \[astro-ph.CO\]](#).
- [89] Pedro Schwaller, “Gravitational Waves from a Dark Phase Transition,” *Phys. Rev. Lett.* **115**, 181101 (2015), [arXiv:1504.07263 \[hep-ph\]](#).
- [90] Amarjit Soni and Yue Zhang, “Gravitational Waves From SU(N) Glueball Dark Matter,” *Phys. Lett. B* **771**, 379–384 (2017), [arXiv:1610.06931 \[hep-ph\]](#).
- [91] Koji Tsumura, Masatoshi Yamada, and Yuya Yamaguchi, “Gravitational wave from dark sector with dark pion,” *JCAP* **07**, 044 (2017), [arXiv:1704.00219 \[hep-ph\]](#).
- [92] Wenyu Wang, Wu-Long Xu, and Jin Min Yang, “A hidden self-interacting dark matter sector with first-order cosmological phase transition and gravitational wave,” *Eur. Phys. J. Plus* **138**, 781 (2023), [arXiv:2209.11408 \[hep-ph\]](#).
- [93] Wenyu Wang, Ke-Pan Xie, Wu-Long Xu, and Jin Min Yang, “Cosmological phase transitions, gravitational waves and self-interacting dark matter in the singlet extension of MSSM,” *Eur. Phys. J. C* **82**, 1120

- (2022), [arXiv:2204.01928 \[hep-ph\]](#).
- [94] Edward Witten, “Cosmic Separation of Phases,” *Phys. Rev. D* **30**, 272–285 (1984).
- [95] Zhaofeng Kang and Jiang Zhu, “Dark Chiral Phase Transition Driven by Chemical Potential and its Gravitational Wave Test,” (2025), [arXiv:2501.15242 \[hep-ph\]](#).
- [96] Francesco Costa, Jaime Hoefken Zink, Michele Lucente, Silvia Pascoli, and Salvador Rosauero-Alcaraz, “Supercooled Dark Scalar Phase Transitions explanation of NANOGrav data,” (2025), [arXiv:2501.15649 \[hep-ph\]](#).
- [97] João Gonçalves, Danny Marfatia, António P. Morais, and Roman Pasechnik, “Supercooled phase transitions in conformal dark sectors explain NANOGrav data,” (2025), [arXiv:2501.11619 \[hep-ph\]](#).
- [98] Jinzheng Li and Pran Nath, “Supercooled Phase Transitions: Why Thermal History of Hidden Sector Matters in Analysis of Pulsar Timing Array Signals,” (2025), [arXiv:2501.14986 \[hep-ph\]](#).
- [99] Amitayus Banik, Yanou Cui, Yu-Dai Tsai, and Yuhsin Tsai, “The Sound of Dark Sectors in Pulsar Timing Arrays,” (2024), [arXiv:2412.16282 \[hep-ph\]](#).
- [100] Yang Bai and Mrunal Korwar, “Cosmological constraints on first-order phase transitions,” *Phys. Rev. D* **105**, 095015 (2022), [arXiv:2109.14765 \[hep-ph\]](#).
- [101] Francis-Yan Cyr-Racine, Roland de Putter, Alvise Raccanelli, and Kris Sigurdson, “Constraints on Large-Scale Dark Acoustic Oscillations from Cosmology,” *Phys. Rev. D* **89**, 063517 (2014), [arXiv:1310.3278 \[astro-ph.CO\]](#).
- [102] Francis-Yan Cyr-Racine and Kris Sigurdson, “Cosmology of atomic dark matter,” *Phys. Rev. D* **87**, 103515 (2013), [arXiv:1209.5752 \[astro-ph.CO\]](#).
- [103] Matthew R. Buckley, Jesús Zavala, Francis-Yan Cyr-Racine, Kris Sigurdson, and Mark Vogelsberger, “Scattering, Damping, and Acoustic Oscillations: Simulating the Structure of Dark Matter Halos with Relativistic Force Carriers,” *Phys. Rev. D* **90**, 043524 (2014), [arXiv:1405.2075 \[astro-ph.CO\]](#).
- [104] Adam Falkowski, Joshua T. Ruderman, and Tomer Volansky, “Asymmetric Dark Matter from Leptogenesis,” *JHEP* **05**, 106 (2011), [arXiv:1101.4936 \[hep-ph\]](#).
- [105] Manoranjan Dutta, Nimmala Narendra, Narendra Sahu, and Sujay Shil, “Asymmetric self-interacting dark matter via Dirac leptogenesis,” *Phys. Rev. D* **106**, 095017 (2022), [arXiv:2202.04704 \[hep-ph\]](#).
- [106] Haipeng An, Shao-Long Chen, Rabindra N. Mohapatra, and Yue Zhang, “Leptogenesis as a Common Origin for Matter and Dark Matter,” *JHEP* **03**, 124 (2010), [arXiv:0911.4463 \[hep-ph\]](#).
- [107] Sean Tulin, Hai-Bo Yu, and Kathryn M. Zurek, “Oscillating Asymmetric Dark Matter,” *JCAP* **05**, 013 (2012), [arXiv:1202.0283 \[hep-ph\]](#).
- [108] Matthew R. Buckley and Stefano Profumo, “Regenerating a Symmetry in Asymmetric Dark Matter,” *Phys. Rev. Lett.* **108**, 011301 (2012), [arXiv:1109.2164 \[hep-ph\]](#).
- [109] Song Li, Jin Min Yang, Mengchao Zhang, and Rui Zhu, “Theoretical bounds on dark Higgs mass in a self-interacting dark matter model with  $U(1)'$ ,” (2024), [arXiv:2405.18226 \[hep-ph\]](#).
- [110] M. Karjalainen, M. Laine, and J. Peisa, “The Order of the phase transition in 3-d  $U(1) +$  Higgs theory,” *Nucl. Phys. B Proc. Suppl.* **53**, 475–480 (1997), [arXiv:hep-lat/9608006](#).
- [111] P. Dimopoulos, K. Farakos, and G. Koutsoumbas, “Three-dimensional lattice  $U(1)$  gauge Higgs model at low  $m(H)$ ,” *Eur. Phys. J. C* **1**, 711–719 (1998), [arXiv:hep-lat/9703004](#).
- [112] Iason Baldes and Kalliopi Petraki, “Asymmetric thermal-relic dark matter: Sommerfeld-enhanced freeze-out, annihilation signals and unitarity bounds,” *JCAP* **09**, 028 (2017), [arXiv:1703.00478 \[hep-ph\]](#).

- [113] Michael L. Graesser, Ian M. Shoemaker, and Luca Vecchi, “Asymmetric WIMP dark matter,” *JHEP* **10**, 110 (2011), [arXiv:1103.2771 \[hep-ph\]](#).
- [114] Torsten Bringmann, Paul Frederik Depta, Thomas Konstandin, Kai Schmidt-Hoberg, and Carlo Tasillo, “Does NANOGrav observe a dark sector phase transition?” *JCAP* **11**, 053 (2023), [arXiv:2306.09411 \[astro-ph.CO\]](#).
- [115] Lars Husdal, “On Effective Degrees of Freedom in the Early Universe,” *Galaxies* **4**, 78 (2016), [arXiv:1609.04979 \[astro-ph.CO\]](#).
- [116] Ayuki Kamada, Manoj Kaplinghat, Andrew B. Pace, and Hai-Bo Yu, “How the Self-Interacting Dark Matter Model Explains the Diverse Galactic Rotation Curves,” *Phys. Rev. Lett.* **119**, 111102 (2017), [arXiv:1611.02716 \[astro-ph.GA\]](#).
- [117] Tao Ren, Anna Kwa, Manoj Kaplinghat, and Hai-Bo Yu, “Reconciling the Diversity and Uniformity of Galactic Rotation Curves with Self-Interacting Dark Matter,” *Phys. Rev. X* **9**, 031020 (2019), [arXiv:1808.05695 \[astro-ph.GA\]](#).
- [118] Manoj Kaplinghat, Tao Ren, and Hai-Bo Yu, “Dark Matter Cores and Cusps in Spiral Galaxies and their Explanations,” *JCAP* **06**, 027 (2020), [arXiv:1911.00544 \[astro-ph.GA\]](#).
- [119] Camila A. Correa, “Constraining velocity-dependent self-interacting dark matter with the Milky Way’s dwarf spheroidal galaxies,” *Mon. Not. Roy. Astron. Soc.* **503**, 920–937 (2021), [arXiv:2007.02958 \[astro-ph.GA\]](#).
- [120] Quinn E. Minor, Sophia Gad-Nasr, Manoj Kaplinghat, and Simona Vegetti, “An unexpected high concentration for the dark substructure in the gravitational lens SDSSJ0946+1006,” *Mon. Not. Roy. Astron. Soc.* **507**, 1662–1683 (2021), [arXiv:2011.10627 \[astro-ph.GA\]](#).
- [121] Ethan O. Nadler, Daneng Yang, and Hai-Bo Yu, “A Self-interacting Dark Matter Solution to the Extreme Diversity of Low-mass Halo Properties,” *Astrophys. J. Lett.* **958**, L39 (2023), [arXiv:2306.01830 \[astro-ph.GA\]](#).
- [122] Felix Kahlhoefer, Kai Schmidt-Hoberg, and Sebastian Wild, “Dark matter self-interactions from a general spin-0 mediator,” *JCAP* **08**, 003 (2017), [arXiv:1704.02149 \[hep-ph\]](#).
- [123] S. A. Khrapak, A. V. Ivlev, G. E. Morfill, and S. K. Zhdanov, “Scattering in the Attractive Yukawa Potential in the Limit of Strong Interaction,” *Phys. Rev. Lett.* **90**, 225002 (2003).
- [124] Francis-Yan Cyr-Racine, Kris Sigurdson, Jesus Zavala, Torsten Bringmann, Mark Vogelsberger, and Christoph Pfrommer, “ETHOS—an effective theory of structure formation: From dark particle physics to the matter distribution of the Universe,” *Phys. Rev. D* **93**, 123527 (2016), [arXiv:1512.05344 \[astro-ph.CO\]](#).
- [125] Brian Colquhoun, Saniya Heeba, Felix Kahlhoefer, Laura Sagunski, and Sean Tulin, “Semiclassical regime for dark matter self-interactions,” *Phys. Rev. D* **103**, 035006 (2021), [arXiv:2011.04679 \[hep-ph\]](#).
- [126] Maria Archidiacono, Deanna C. Hooper, Riccardo Murgia, Sebastian Bohr, Julien Lesgourgues, and Matteo Viel, “Constraining Dark Matter-Dark Radiation interactions with CMB, BAO, and Lyman- $\alpha$ ,” *JCAP* **10**, 055 (2019), [arXiv:1907.01496 \[astro-ph.CO\]](#).
- [127] Pablo F. de Salas and Sergio Pastor, “Relic neutrino decoupling with flavour oscillations revisited,” *JCAP* **07**, 051 (2016), [arXiv:1606.06986 \[hep-ph\]](#).
- [128] Carroll Wainwright, Stefano Profumo, and Michael J. Ramsey-Musolf, “Gravity Waves from a Cosmological Phase Transition: Gauge Artifacts and Daisy Resummations,” *Phys. Rev. D* **84**, 023521 (2011), [arXiv:1104.5487 \[hep-ph\]](#).

- [129] Cheng-Wei Chiang and Eibun Senaha, “On gauge dependence of gravitational waves from a first-order phase transition in classical scale-invariant  $U(1)'$  models,” *Phys. Lett. B* **774**, 489–493 (2017), [arXiv:1707.06765 \[hep-ph\]](#).
- [130] Sidney R. Coleman and Erick J. Weinberg, “Radiative Corrections as the Origin of Spontaneous Symmetry Breaking,” *Phys. Rev. D* **7**, 1888–1910 (1973).
- [131] Cedric Delaunay, Christophe Grojean, and James D. Wells, “Dynamics of Non-renormalizable Electroweak Symmetry Breaking,” *JHEP* **04**, 029 (2008), [arXiv:0711.2511 \[hep-ph\]](#).
- [132] Greg W. Anderson and Lawrence J. Hall, “The Electroweak phase transition and baryogenesis,” *Phys. Rev. D* **45**, 2685–2698 (1992).
- [133] L. Dolan and R. Jackiw, “Symmetry Behavior at Finite Temperature,” *Phys. Rev. D* **9**, 3320–3341 (1974).
- [134] Mariano Quiros, “Finite temperature field theory and phase transitions,” in *ICTP Summer School in High-Energy Physics and Cosmology* (1999) pp. 187–259, [arXiv:hep-ph/9901312](#).
- [135] Peter Brockway Arnold and Olivier Espinosa, “The Effective potential and first order phase transitions: Beyond leading-order,” *Phys. Rev. D* **47**, 3546 (1993), [Erratum: *Phys.Rev.D* 50, 6662 (1994)], [arXiv:hep-ph/9212235](#).
- [136] Alan H. Guth and Erick J. Weinberg, “Cosmological Consequences of a First Order Phase Transition in the  $SU(5)$  Grand Unified Model,” *Phys. Rev. D* **23**, 876 (1981).
- [137] Alan H. Guth and S. H. H. Tye, “Phase Transitions and Magnetic Monopole Production in the Very Early Universe,” *Phys. Rev. Lett.* **44**, 631 (1980), [Erratum: *Phys.Rev.Lett.* 44, 963 (1980)].
- [138] Ariel Megevand and Santiago Ramirez, “Bubble nucleation and growth in very strong cosmological phase transitions,” *Nucl. Phys. B* **919**, 74–109 (2017), [arXiv:1611.05853 \[astro-ph.CO\]](#).
- [139] Michael S. Turner, Erick J. Weinberg, and Lawrence M. Widrow, “Bubble nucleation in first order inflation and other cosmological phase transitions,” *Phys. Rev. D* **46**, 2384–2403 (1992).
- [140] Archil Kobakhidze, Cyril Lagger, Adrian Manning, and Jason Yue, “Gravitational waves from a supercooled electroweak phase transition and their detection with pulsar timing arrays,” *Eur. Phys. J. C* **77**, 570 (2017), [arXiv:1703.06552 \[hep-ph\]](#).
- [141] John Ellis, Marek Lewicki, and José Miguel No, “On the Maximal Strength of a First-Order Electroweak Phase Transition and its Gravitational Wave Signal,” *JCAP* **04**, 003 (2019), [arXiv:1809.08242 \[hep-ph\]](#).
- [142] Xiao Wang, Fa Peng Huang, and Xinmin Zhang, “Phase transition dynamics and gravitational wave spectra of strong first-order phase transition in supercooled universe,” *JCAP* **05**, 045 (2020), [arXiv:2003.08892 \[hep-ph\]](#).
- [143] Rong-Gen Cai, Misao Sasaki, and Shao-Jiang Wang, “The gravitational waves from the first-order phase transition with a dimension-six operator,” *JCAP* **08**, 004 (2017), [arXiv:1707.03001 \[astro-ph.CO\]](#).
- [144] Sidney R. Coleman, “The Fate of the False Vacuum. 1. Semiclassical Theory,” *Phys. Rev. D* **15**, 2929–2936 (1977), [Erratum: *Phys.Rev.D* 16, 1248 (1977)].
- [145] Curtis G. Callan, Jr. and Sidney R. Coleman, “The Fate of the False Vacuum. 2. First Quantum Corrections,” *Phys. Rev. D* **16**, 1762–1768 (1977).
- [146] Andrei D. Linde, “Decay of the False Vacuum at Finite Temperature,” *Nucl. Phys. B* **216**, 421 (1983), [Erratum: *Nucl.Phys.B* 223, 544 (1983)].
- [147] Riccardo Apreda, Michele Maggiore, Alberto Nicolis, and Antonio Riotto, “Gravitational waves from electroweak phase transitions,” *Nucl. Phys. B* **631**, 342–368 (2002), [arXiv:gr-qc/0107033](#).

- [148] Carroll L. Wainwright, “CosmoTransitions: Computing Cosmological Phase Transition Temperatures and Bubble Profiles with Multiple Fields,” *Comput. Phys. Commun.* **183**, 2006–2013 (2012), [arXiv:1109.4189 \[hep-ph\]](#).
- [149] Peter Athron, Csaba Balazs, Andrew Fowlie, Lachlan Morris, William Searle, Yang Xiao, and Yang Zhang, “PhaseTracer2: from the effective potential to gravitational waves,” (2024), [arXiv:2412.04881 \[astro-ph.CO\]](#).
- [150] Jose R. Espinosa, Thomas Konstandin, Jose M. No, and Geraldine Servant, “Energy Budget of Cosmological First-order Phase Transitions,” *JCAP* **06**, 028 (2010), [arXiv:1004.4187 \[hep-ph\]](#).
- [151] Dietrich Bodeker and Guy D. Moore, “Electroweak Bubble Wall Speed Limit,” *JCAP* **05**, 025 (2017), [arXiv:1703.08215 \[hep-ph\]](#).
- [152] Mark Hindmarsh, Stephan J. Huber, Kari Rummukainen, and David J. Weir, “Numerical simulations of acoustically generated gravitational waves at a first order phase transition,” *Phys. Rev. D* **92**, 123009 (2015), [arXiv:1504.03291 \[astro-ph.CO\]](#).
- [153] Kai Schmitz, “New Sensitivity Curves for Gravitational-Wave Signals from Cosmological Phase Transitions,” *JHEP* **01**, 097 (2021), [arXiv:2002.04615 \[hep-ph\]](#).
- [154] Guy D. Moore and Tomislav Prokopec, “How fast can the wall move? A Study of the electroweak phase transition dynamics,” *Phys. Rev. D* **52**, 7182–7204 (1995), [arXiv:hep-ph/9506475](#).
- [155] Ariel Megevand and Alejandro D. Sanchez, “Velocity of electroweak bubble walls,” *Nucl. Phys. B* **825**, 151–176 (2010), [arXiv:0908.3663 \[hep-ph\]](#).
- [156] Stephan J. Huber and Miguel Sopena, “An efficient approach to electroweak bubble velocities,” (2013), [arXiv:1302.1044 \[hep-ph\]](#).
- [157] Thomas Konstandin, Germano Nardini, and Ingo Rues, “From Boltzmann equations to steady wall velocities,” *JCAP* **09**, 028 (2014), [arXiv:1407.3132 \[hep-ph\]](#).
- [158] Glauber C. Dorsch, Stephan J. Huber, and Thomas Konstandin, “Bubble wall velocities in the Standard Model and beyond,” *JCAP* **12**, 034 (2018), [arXiv:1809.04907 \[hep-ph\]](#).
- [159] Benoit Laurent and James M. Cline, “First principles determination of bubble wall velocity,” *Phys. Rev. D* **106**, 023501 (2022), [arXiv:2204.13120 \[hep-ph\]](#).
- [160] Xiao Wang, Fa Peng Huang, and Xinmin Zhang, “Bubble wall velocity beyond leading-log approximation in electroweak phase transition,” (2020), [arXiv:2011.12903 \[hep-ph\]](#).
- [161] Marc Kamionkowski, Arthur Kosowsky, and Michael S. Turner, “Gravitational radiation from first order phase transitions,” *Phys. Rev. D* **49**, 2837–2851 (1994), [arXiv:astro-ph/9310044](#).
- [162] Arthur Kosowsky, Michael S. Turner, and Richard Watkins, “Gravitational radiation from colliding vacuum bubbles,” *Phys. Rev. D* **45**, 4514–4535 (1992).
- [163] Arthur Kosowsky and Michael S. Turner, “Gravitational radiation from colliding vacuum bubbles: envelope approximation to many bubble collisions,” *Phys. Rev. D* **47**, 4372–4391 (1993), [arXiv:astro-ph/9211004](#).
- [164] Arthur Kosowsky, Michael S. Turner, and Richard Watkins, “Gravitational waves from first order cosmological phase transitions,” *Phys. Rev. Lett.* **69**, 2026–2029 (1992).
- [165] Chiara Caprini, Ruth Durrer, and Geraldine Servant, “Gravitational wave generation from bubble collisions in first-order phase transitions: An analytic approach,” *Phys. Rev. D* **77**, 124015 (2008), [arXiv:0711.2593 \[astro-ph\]](#).

- [166] Stephan J. Huber and Thomas Konstandin, “Gravitational Wave Production by Collisions: More Bubbles,” *JCAP* **09**, 022 (2008), [arXiv:0806.1828 \[hep-ph\]](#).
- [167] Mark Hindmarsh, Stephan J. Huber, Kari Rummukainen, and David J. Weir, “Gravitational waves from the sound of a first order phase transition,” *Phys. Rev. Lett.* **112**, 041301 (2014), [arXiv:1304.2433 \[hep-ph\]](#).
- [168] John T. Giblin and James B. Mertens, “Gravitational radiation from first-order phase transitions in the presence of a fluid,” *Phys. Rev. D* **90**, 023532 (2014), [arXiv:1405.4005 \[astro-ph.CO\]](#).
- [169] John T. Giblin, Jr. and James B. Mertens, “Vacuum Bubbles in the Presence of a Relativistic Fluid,” *JHEP* **12**, 042 (2013), [arXiv:1310.2948 \[hep-th\]](#).
- [170] Chiara Caprini and Ruth Durrer, “Gravitational waves from stochastic relativistic sources: Primordial turbulence and magnetic fields,” *Phys. Rev. D* **74**, 063521 (2006), [arXiv:astro-ph/0603476](#).
- [171] Tina Kahniashvili, Leonardo Campanelli, Grigol Gogoberidze, Yurii Maravin, and Bharat Ratra, “Gravitational Radiation from Primordial Helical Inverse Cascade MHD Turbulence,” *Phys. Rev. D* **78**, 123006 (2008), [Erratum: *Phys.Rev.D* 79, 109901 (2009)], [arXiv:0809.1899 \[astro-ph\]](#).
- [172] Tina Kahniashvili, Arthur Kosowsky, Grigol Gogoberidze, and Yurii Maravin, “Detectability of Gravitational Waves from Phase Transitions,” *Phys. Rev. D* **78**, 043003 (2008), [arXiv:0806.0293 \[astro-ph\]](#).
- [173] Tina Kahniashvili, Leonard Kisslinger, and Trevor Stevens, “Gravitational Radiation Generated by Magnetic Fields in Cosmological Phase Transitions,” *Phys. Rev. D* **81**, 023004 (2010), [arXiv:0905.0643 \[astro-ph.CO\]](#).
- [174] Chiara Caprini, Ruth Durrer, and Geraldine Servant, “The stochastic gravitational wave background from turbulence and magnetic fields generated by a first-order phase transition,” *JCAP* **12**, 024 (2009), [arXiv:0909.0622 \[astro-ph.CO\]](#).
- [175] Leonard Kisslinger and Tina Kahniashvili, “Polarized Gravitational Waves from Cosmological Phase Transitions,” *Phys. Rev. D* **92**, 043006 (2015), [arXiv:1505.03680 \[astro-ph.CO\]](#).
- [176] Chiara Caprini *et al.*, “Science with the space-based interferometer eLISA. II: Gravitational waves from cosmological phase transitions,” *JCAP* **04**, 001 (2016), [arXiv:1512.06239 \[astro-ph.CO\]](#).
- [177] Chiara Caprini *et al.*, “Detecting gravitational waves from cosmological phase transitions with LISA: an update,” *JCAP* **03**, 024 (2020), [arXiv:1910.13125 \[astro-ph.CO\]](#).
- [178] Gemma Janssen *et al.*, “Gravitational wave astronomy with the SKA,” *PoS AASKA14*, 037 (2015), [arXiv:1501.00127 \[astro-ph.IM\]](#).
- [179] Pau Amaro-Seoane *et al.* (LISA), “Laser Interferometer Space Antenna,” (2017), [arXiv:1702.00786 \[astro-ph.IM\]](#).
- [180] Eric Thrane and Joseph D. Romano, “Sensitivity curves for searches for gravitational-wave backgrounds,” *Phys. Rev. D* **88**, 124032 (2013), [arXiv:1310.5300 \[astro-ph.IM\]](#).